# LOAN DOCUMENT

PHOTOGRAPH THIS SHEET

DTIC ACCESSION NUMBER

LEVEL

INVENTORY

Cutting Force Measurement in Production . . .

DOCUMENT IDENTIFICATION

May 80

DISTRIBUTION STATEMENT A
Approved for public release;
Distribution Unlimited

DISTRIBUTION STATEMENT

ACCESSION FOR

| | | |
|---|---|---|
| NTIS | GRA&I | ☑ |
| DTIC | TRAC | ☐ |
| UNANNOUNCED | | ☐ |
| JUSTIFICATION | | |

BY

DISTRIBUTION/

AVAILABILITY CODES

| DISTRIBUTION | AVAILABILITY AND/OR SPECIAL | |
|---|---|---|
| A-1 | | |

DISTRIBUTION STAMP

DATE ACCESSIONED

DATE RETURNED

DTIC QUALITY INSPECTED 1

19970226 128

DATE RECEIVED IN DTIC

REGISTERED OR CERTIFIED NUMBER

PHOTOGRAPH THIS SHEET AND RETURN TO DTIC-FDAC

HANDLE WITH CARE

DTIC FORM 70A JUN 90

DOCUMENT PROCESSING SHEET

PREVIOUS EDITIONS MAY BE USED UNTIL STOCK IS EXHAUSTED.

LOAN DOCUMENT

6 MAR 1997

TL

RIA-81-U55

PB80-208291

# Cutting Force Measurement in Production Machining via Instrumented Toolholders



Advanced Mechanical Technology, Inc.
Newton, MA

Prepared for

National Science Foundation
Washington, DC

May 80

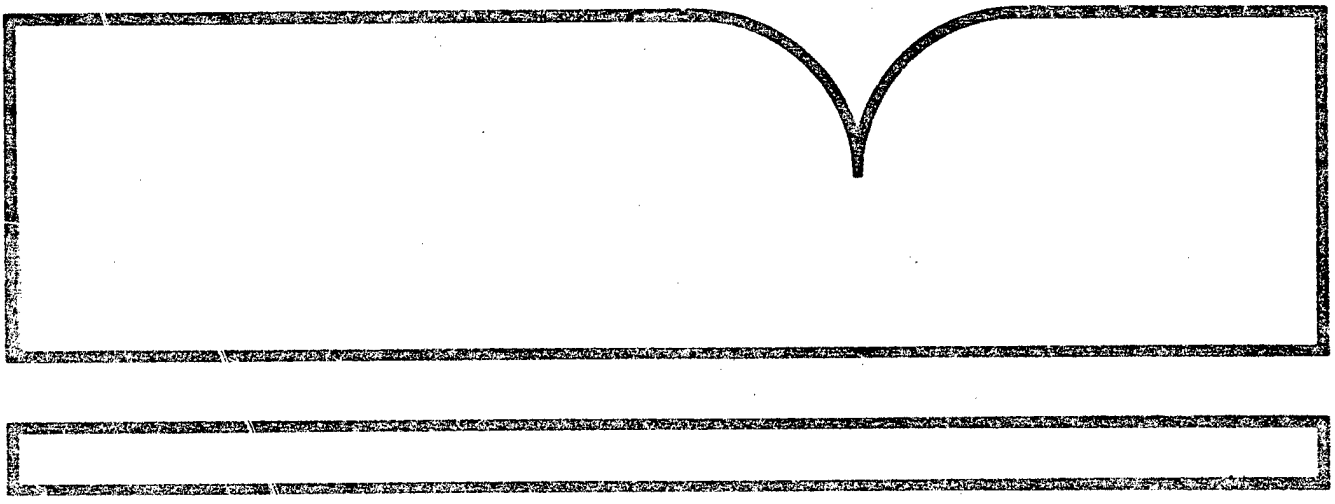

U.S. Department of Commerce
National Technical Information Service
NTIS

# DISCLAIMER NOTICE

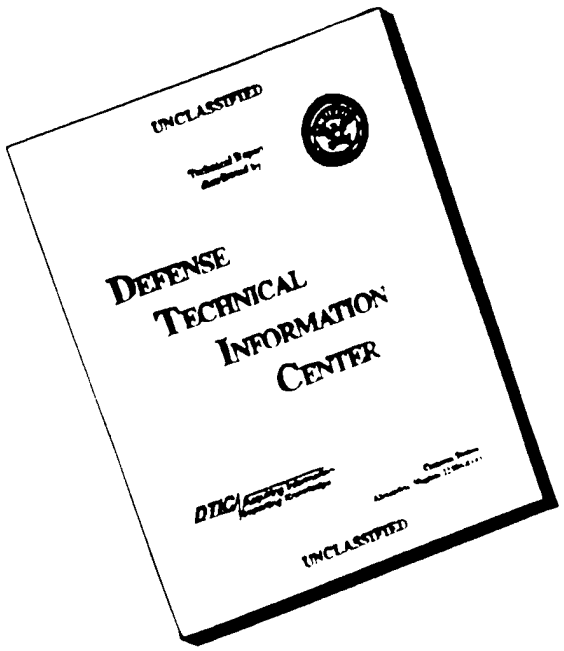


**THIS DOCUMENT IS BEST QUALITY AVAILABLE. THE COPY FURNISHED TO DTIC CONTAINED A SIGNIFICANT NUMBER OF PAGES WHICH DO NOT REPRODUCE LEGIBLY.**

# CUTTING FORCE MEASUREMENT IN PRODUCTION MACHINING VIA INSTRUMENTED TOOLHOLDERS

PHASE I - FINAL REPORT

John F. Pearson
Walter D. Syniuta
Nathan H. Cook

Contract No. NSF DAR-7917156

ADVANCED MECHANICAL TECHNOLOGY, INC.
141 CALIFORNIA STREET • NEWTON, MASSACHUSETTS 02158 • (617) 964-2042
TELEX 710-335-0406

50272-101

| REPORT DOCUMENTATION PAGE | 1. REPORT NO. NSF/RA-800081 | 2. | 3. Recipient's Accession No. PB80 208291 |
|---|---|---|---|

**4. Title and Subtitle**
Cutting Force Measurement in Production Machining Via Instrumented Toolholders, Phase I - Fina' Report

**5. Report Date**
May 1980

**6.**

**7. Author(s)**
J. F. Pearson, W. D. Syniuta, N.H. Cook

**8. Performing Organization Rept. No**

**9. Performing Organization Name and Address**
Advanced Mechanical Technology, Inc.
141 California Street
Newton, MA 02158

**10. Project/Task/Work Unit No.**

**11. Contract(C) or Grant(G) No.**
(C)
(G) DAR7917156

**12. Sponsoring Organization Name and Address**
Engineering and Applied Science (EAS)
National Science Foundation
1800 G Street, N.W.
Washington, D.C. 20550

**13. Type of Report & Period Covered**
Final
Phase I

**14.**

**15. Supplementary Notes**

**16. Abstract (Limit: 200 words)**

This report describes the development of a low-cost metal cutting force transducer which accurately predicts the magnitude of strain signals on an instrumental standard lathe toolholder. This innovative approach to the measurement of cutting tool forces is critical to developing "adaptive control" machining capable of dramatically improving national productivity and conserving energy and materials. A gage mounting design model with three prototype configurations was proposed and validated by computer analysis. The prototype constructed followed the analytical model within size constraints. The initial model tested acceptably for the measurement of vertical and horizontal force components, but the axial measurement showed considerable thermal instability. Accordingly, the gage monitoring scheme was modified to reduce thermal drift. A series of calibration tests established system sensitivity and linearity, and a series of lathe cutting tests validated the functionality of the instrumented toolholder system. Several options for systems application were defined including force monitoring and input to a computer-numeric-controlled system.

**17. Document Analysis a. Descriptors**

Lathes
Transducers
Cutting tools
Adaptive systems
Calibrating
Cost effectiveness
Measuring instruments
Automatic control equipment

**b. Identifiers/Open-Ended Terms**

Toolholders

**c. COSATI Field/Group**

Applied Physical, Mathematical, and Biological Sciences, and Engineering

| 18. Availability Statement | 19. Security Class (This Report) | 21. No. of Pages |
|---|---|---|
| NTIS | 20. Security Class (This Page) | 22. Price |

(See ANSI-Z39.18) See Instructions on Reverse

OPTIONAL FORM 272 (4-77)
(Formerly NTIS-35)
Department of Commerce

May 30, 1980

# CUTTING FORCE MEASUREMENT IN PRODUCTION MACHINING VIA INSTRUMENTED TOOLHOLDERS

PHASE I - FINAL REPORT

John F. Pearson
Walter D. Syniuta
Nathan H. Cook

Contract No. NSF DAR-7917156

Prepared for:

NATIONAL SCIENCE FOUNDATION

Division of Applied Research/EAS

Washington, D. C. 20550

By

Advanced Mechanical Technology Incorporated
141 California Street
Newton, Massachusetts 02158

This research was conducted with the support of the National Science Foundation. However, any opinions, findings, conclusions or recommendations expressed in this report are those of the authors and do not necessarily reflect the views of the National Science Foundation.

TABLE OF CONTENTS

## LIST OF FIGURES

## LIST OF TABLES

## LIST OF SYMBOLS

| Symbol | | |
|---|---|---|
| $a$ | y-coordinate of cutting point M | in |
| $a_{11}, a_{12}, \ldots, a_{33}$ | coefficients relating strains to forces | |
| $A_{csx}$ | crossectional area of toolholder | $in^2$ |
| $b$ | base of toolholder shank | in |
| $b_{11}, b_{12}, \ldots, b_{33}$ | influence coefficients relating channel outputs to forces | |
| $b'_{11}, b'_{12}, \ldots, b'_{33}$ | coefficients relating forces to channel outputs | |
| $[B]$ | matrix of $b'_{ij}$ coefficients above | |
| $c$ | x-coordinate of cutting point M | in |
| $E$ | modulus of elasticity | $bf/in^2$ |
| $[F]$ | matrix of force components | lbf |
| $F_p, F_q, F_r$ | vertical, horizontal and axial force components | lbf |
| FS | full-scale (abbreviation) | |
| $h$ | height of toolholder shank | in |
| $I_{xx}, I_{yy}$ | moment of inertia about x and y-axes | $in^4$ |
| $l$ | distance from cutting point M to gage sites | in |
| $L$ | distance from cutting point M to clamping plane | in |
| $M_x, M_y, M_z$ | bending moments about x, y, z-axes | lbf |
| $P$ | power dissipation | watt |
| $P_1, P_2$ | points defined by Fig. 5 | |

| | | |
|---|---|---|
| R | electrical resistance | ohm |
| RTO | referred to output (abbreviation) | |
| S | gage factor (abbreviated GF) | |
| $V_1$ $V_2$, $V_3$ | matrix of channel outputs | |
| [V] | channel outputs | volt |
| $V_{b_1}$, $V_{b_2}$, $V_{b_3}$ | bridge excitation voltages | volt |
| $V_{out\ 1}$, $V_{out\ 2}$, $V_{out\ 3}$ | bridge output voltages | volt |
| x, y, z | coordinates of Cartesian system | |
| $\beta$ | angle of inclination of neutral plane | degree |
| $\varepsilon_n$ | strain at position n | |

# 1. SUMMARY OF PHASE I ACCOMPLISHMENTS

The primary objective of Phase I research program was to demonstrate the feasibility of instrumenting a standard lathe toolholder with strain gages as a means of producing a low-cost cutting force transducer. The two tasks identified as critical in this proof-of-concept program were

1. Develop a strain gage mounting scheme which would maximize sensitivity and permit isolation of individual force components.
2. Develop signal conditioning and processing methods to interface the instrumented toolholder with the variety of likely applications.

A gage mounting scheme was developed which provided suitable sensitivity and force component isolation. A computer analysis was performed to investigate the validity of this methodology and to model three proposed prototype configurations. Analytical results indicated that any of the three would result in a successful transducer design.

A prototype was constructed which followed the analytical model within the constraints of size. This initial model was tested and found acceptable for the measurement of vertical and horizontal force components. The axial measurement showed considerable thermal instability. The gage mounting scheme for measuring axial force was modified to reduce thermal drift. This second version showed greatly improved thermal performance, though still falling short of system design requirements.

A series of calibration tests were performed to establish system

sensitivity and linearity. These tests resulted in excellent sensitivity and linearity in the vertical and horizontal directions.

A series of lathe cutting tests were performed to establish the functionality of the Instrumented Toolholder System. Measurements made on a standard lathe and in conjunction with a research dynamometer verified that the system operated in a reliable and adequate fashion.

Several options for system applications were defined which included force monitoring and input to a computer-numeric-controlled system. A signal conditioning/processing scheme was identified for each of these options. Preliminary design considerations were established which outline the requirements for these options.

## 2. RECOMMENDATIONS FOR PHASE II RESEARCH

The Phase I feasibility research established that it is possible to obtain accurate cutting force measurements with a standard toolholder by using conventional strain gages with appropriate signal processing. Further research is required in four main areas before the technique can be applied as a practical tool wear measurement system. The major research tasks are as follows:

1. Develop Practical Transducer Design Techniques: In addition to solving the problem of measuring axial forces with the same level of precision and sensitivity as the horizontal and vertical forces, the gaging technique must be ruggedized without excessive loss of sensitivity and accuracy so that the instrumented toolholder can withstand the rigors of industrial use. This work should be brought to the stage where a ruggedized prototype can be tested in an actual industrial environment.

2. Define Correlation Techniques: In order for a practical system to result from the proposed research, the information obtained in the cutting force signals must be translated into the desired knowledge about the tool/workpiece system. Out of the large number of correlations available, e.g., absolute force levels, ratios of two or three force components, etc., the one or two techniques that hold the most promise in terms of accuracy, widespread applicability, cost effectiveness, etc., should be identified and appropriate information processing techniques should be developed.

3. Identify Interface with NC Machines: While it is generally acknowledged that knowledge of cutting conditions is necessary for adaptive control of NC machines, it is not clear how the NC machine should utilize this information, nor how interface should be defined. While there is probably no unique answer to this question, one or more promising adaptive control applications should be identified and researched in order to establish that tool force measurement can indeed provide useful input to adaptive control machining.

4. Field Test Tool Force Measurement System: The outputs of the first three tasks should be tested through field evaluation of a prototype system employing a ruggedized, instrumented toolholder (Task 1), a prototype signal processing package (Task 2), to provide input for adaptive control of a CNC control machining system (Task 3).

# 3. GENERAL REQUIREMENTS FOR INSTRUMENTED TOOLHOLDER DESIGN

## 3.1 Introduction

An important national problem is the slipping productivity in the U.S. relative to other countries. Computer controlled machining is fast becoming a larger part of small batch manufacturing machining capacity. The next step beyond this phase, which can provide a tremendous improvement in productivity, and result in energy and material conservation is "adaptive control" machining. However, this step would require the development of an inexpensive innovative approach to measurement of cutting tool forces. The force components can then be fed back to the computer and used to optimize the machine process.

The major force components acting on a cutting tool vary in magnitude, phase, and ratio according to many conditions such as: flank wear, sharpness of the cutting edge, workpiece rigidity, cooling effectiveness, etc. A reliable, inexpensive, non-obtrusive, non-invasive production-type tool

force sensor would provide the missing link required for adaptive control machining. Furthermore, even without adaptive control, the output of such a sensor can be used to monitor tool wear, breakage, workpiece condition, etc., and thus can provide important benefits in and of itself.

The forces involved in metal-cutting operations have been measured for many years by those involved in cutting research. It has been clear that monitoring cutting forces can provide signals rich in information on tool condition, vibration, tolerance, machine utilization, etc. However, the use of cutting force measurement in production control has been severely limited due to the nature of the force dynamometers available. Most dynamometers are primarily suited to research activity and do not have the operational flexibility or low cost required for use in a general purpose machining environment; i.e., it is not practical to interpose an extra electro-mechanical device between the machine structure and the cutting tool.

A satisfactory production-oriented dynamometer must be such that it in no way interferes with the "normal" operation of the machine-tool. Conceptually, some part of the standard machine structure could be instrumented in a manner to give force information. This, if possible, would have to be done by a machine-tool builder.

In recent years, there has been a growing tendency to use some form of "toolholder" between the machine-tool and the actual cutter. In turning operations, for instance, the common practice is to employ a toolholder which supports disposable cutting inserts of tungsten-carbide, ceramic,

other tool material. Fig. 1 shows a typical lathe toolholder.

The goal of the Phase I research has been to explore the feasibility of the instrumented toolholders to serve as cutting force dynamometers. This method will provide the necessary force signals while permitting normal operation of the machine/tool system.

## 3.2 Discussion of Matrix Methods for Instrumented Toolholder Force Resolution

In order to appreciate the design problems, consider a typical cantilever beam-type two-force component lathe dynamometer as shown in Fig. 2a. The design is such that the point of force application lies on the neutral axis of the beam (z-axis). Gages are placed symmetrically on four sides of the beam to measure moments about the X and Y axes, and therefore the forces producing those moments. Because the point of force application is on the Z axis, the moment about the X axis is due only to $F_p$ and that about the Y axis to $F_q$, and $F_r$ has no effect at all.

Fig. 2b shows the geometry associated with most standard lathe toolholders; the p oint of force application (M) is offset from the Z axis by a and c. In this instance the radial force $F_r$ affects $M_x$ and $M_y$; and both $F_p$ and $F_q$ apply twisting moments about the Z axis. Thus,any strain gages applied to the toolholder will be sensitive to at least two of the applied forces.

Theoretically, 3 strain gages randomly placed on a toolholder would provide enough information to determine the force components. However, from

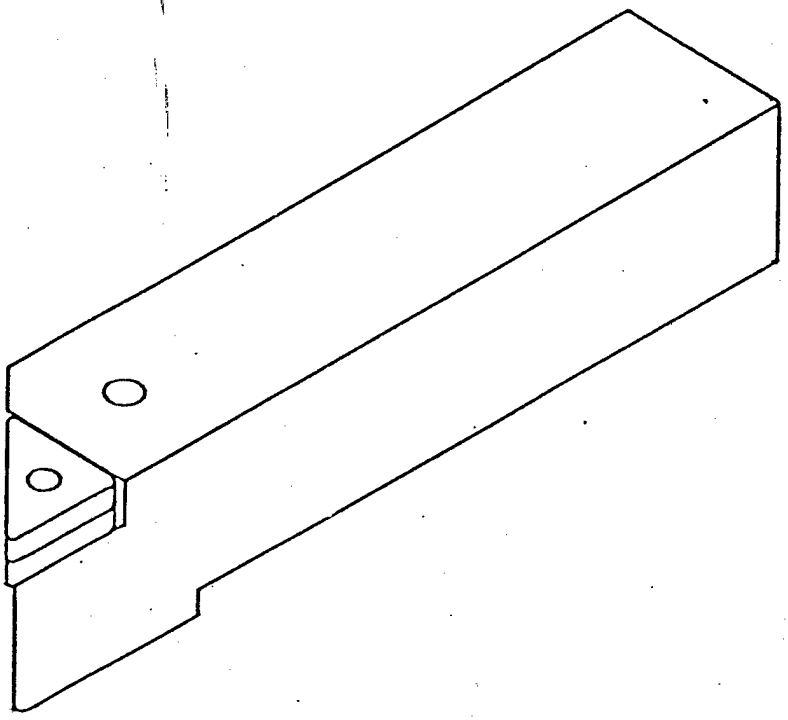

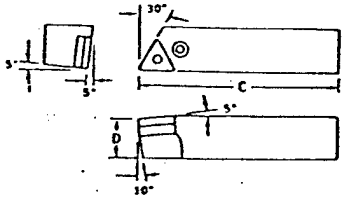


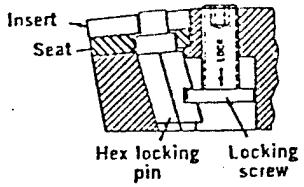


FIGURE 1: A TYPICAL TOOLHOLDER FOR LATHE OPERATION

3-Component Dynamometer

$F_p$ — vertical cutting force
$F_q$ — axial thrust (feed) force
$F_r$ — radial force

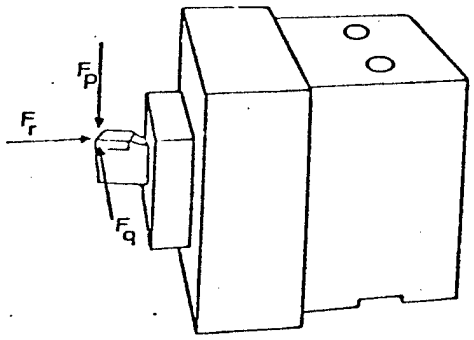


FIGURE 2a: TYPICAL CANTILEVER BEAM-TYPE LATHE DYNAMOMETER

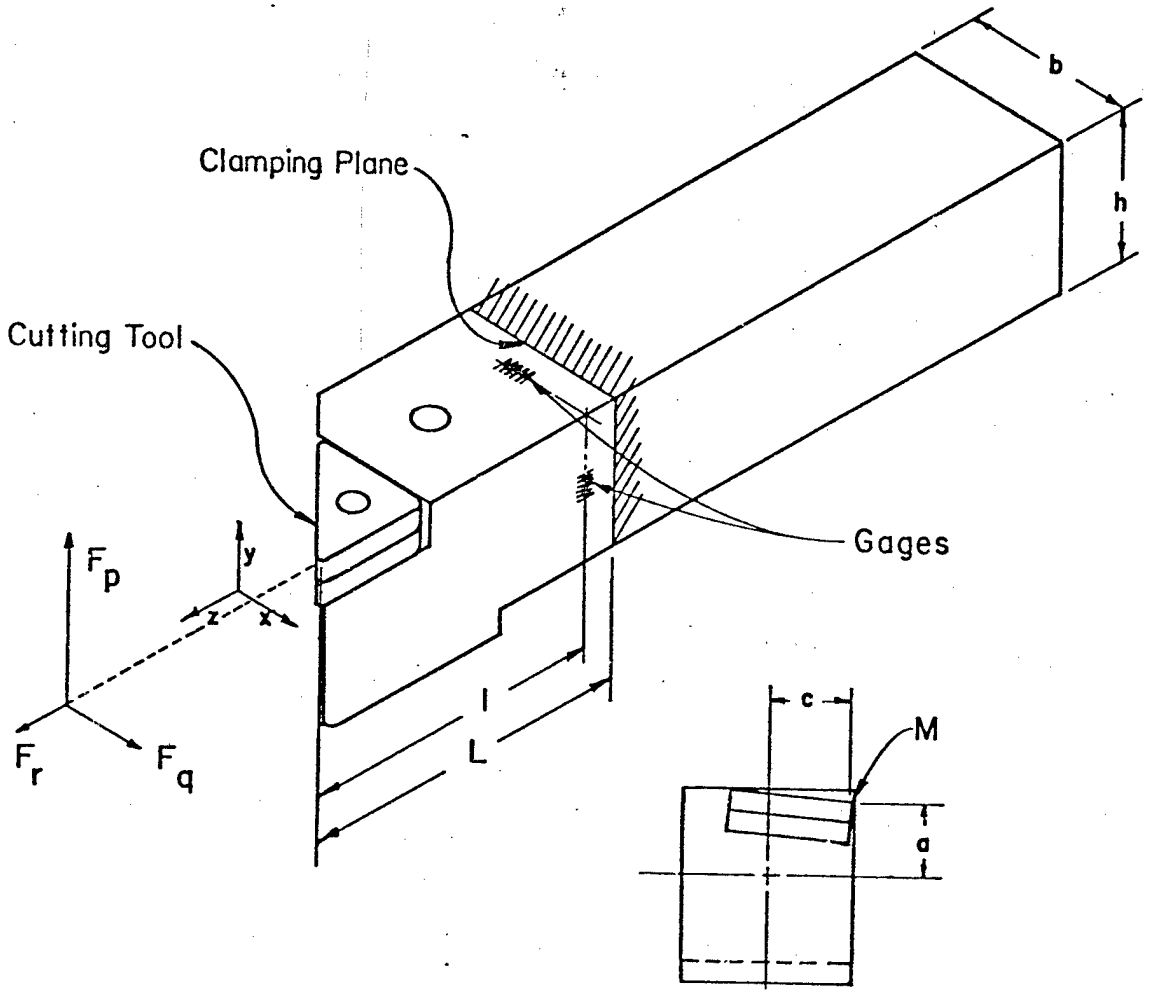


FIGURE 2b: BASIC TOOLHOLDER GEOMETRY

a practical point of view, we know there must be an optimal set of gage locations which will give the least overall error.

In order to use such a device, we will have to determine an influence-matrix that defines this relationship between each output and each force component. To express this analytically, if the three desired force components are $F_1$, $F_2$, $F_3$; and the three strain gage readings are $V_1$, $V_2$, $V_3$, then we can reasonably assume a linear relationship such that:

$$F_1 = b_{11}V_1 + b_{12}V_2 + b_{13}V_3$$

$$F_2 = b_{21}V_1 + b_{22}V_2 + b_{23}V_3$$

$$F_3 = b_{31}V_1 + b_{32}V_2 + b_{33}V_3$$

or

$$\begin{bmatrix} F_1 \\ F_2 \\ F_3 \end{bmatrix} = [B] \begin{bmatrix} V_1 \\ V_2 \\ V_3 \end{bmatrix}$$

where [B] is the influence-matrix:

$$\begin{matrix} b_{11} & b_{12} & b_{13} \\ b_{21} & b_{22} & b_{23} \\ b_{31} & b_{32} & b_{33} \end{matrix}$$

For an ideal dynamometer (such as we build for research purposes) only the main diagonal terms ($b_{11}$, $b_{22}$, $b_{33}$) are significant, the others being essentially (and desirably) zero. For the instrumented toolholder, it will not be possible for all off diagonal terms to be zero. However, with optimal

gage location, we are able to make the diagonal terms dominant so that when the matrix multiplication is carried out, the inevitable measurement errors will not affect the system accuracy significantly.

### 3.3 Brief Discussion of the Major Elements of the Instrumented Toolholder System

A brief description of the instrumented toolholder system follows. In Figure 3 the three basic elements of the instrumented toolholder force transducer are illustrated. The first element, the prototype toolholder device is instrumented with strain gages and generates low level output signals. The second element is a signal conditioner which provides bridge excitation voltage to the toolholder strain gages and amplifies the bridge output signals such that the resultant force signals are ready for matrix manipulation. The third and final element is the analog electronic circuit which performs the matrix manipulation and directly displays the horizontal, vertical and radial forces which have been applied to the instrumented toolholder. Digital indication of three orthogonal forces can be displayed in real time to give a lathe operator visual indication of the work which his lathe tool bit is performing.

## 4. TRANSDUCER DESIGN

In this section we shall address the design of the prototype instrumented toolholder. We shall begin by looking at strain gage mounting schemes which will permit high sensitivity and force-component measurement

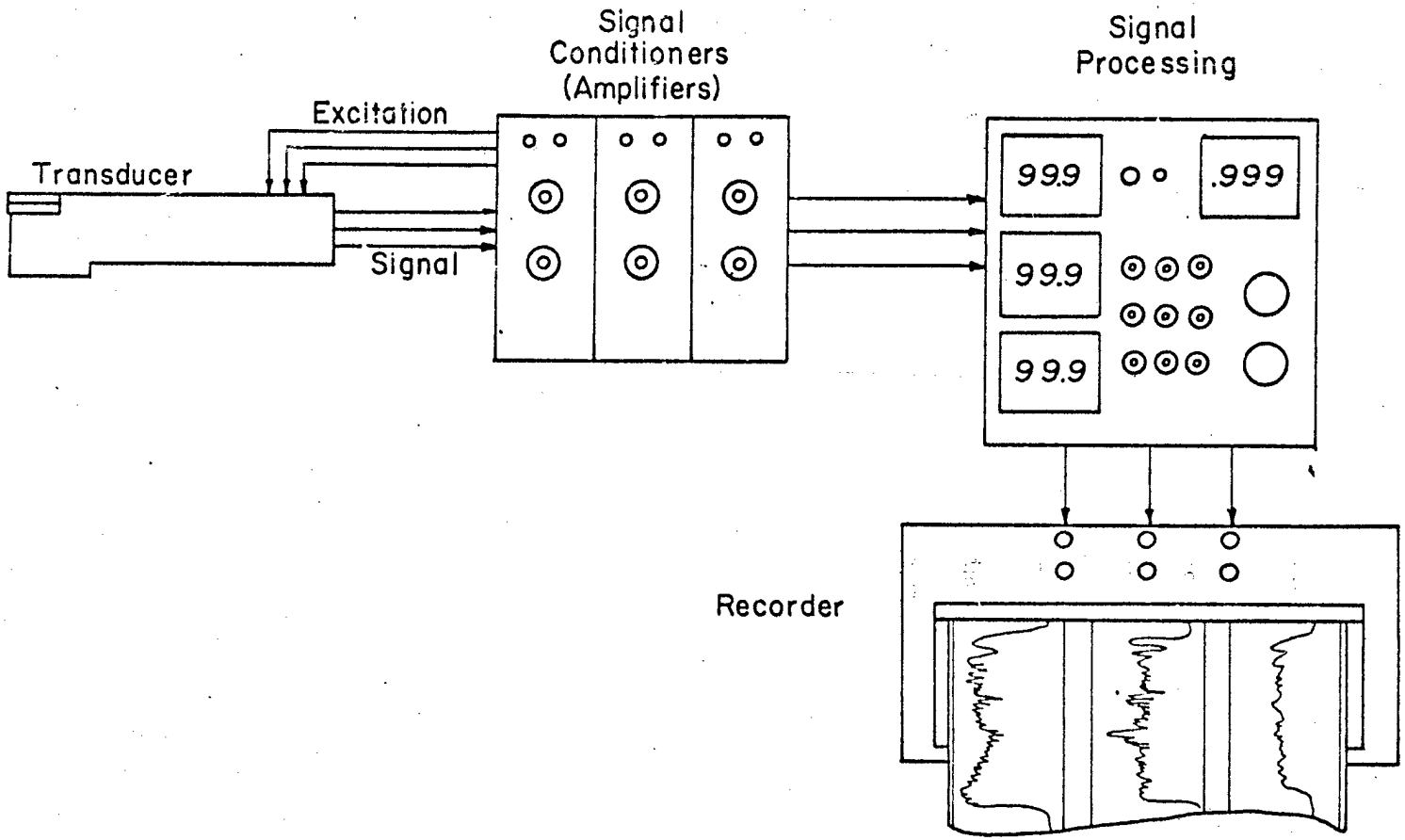


FIGURE 3: INSTRUMENTED TOOLHOLDER PROTOTYPE SYSTEM COMPONENTS

isolation (Thus minimizing the off diagonal terms in the influence matrix.). This methodology will permit us to generate a set of gage positions to satisfy the design criteria of maximum sensitivity and force component isolation. These gage locations will then permit the development of an analytical model for predicting transducer performance.

## 4.1 Optimization of Strain Gage Placement

Figure 2b represents a typical toolholder for a turning process. The cutting point M experiences a force which can be resolved into three orthogonal components, $F_p$, $F_q$ and $F_r$. The toolholder is clamped in a tool post a distance L from the cutting point.

### 4.1.1 Vertical and Horizontal Force Components, $F_p$ and $F_q$

Some conclusions about optimizing strain gage location for force measurement can be reached through some simple observations. First of all, in order to choose a location which will maximize sensitivity to $F_p$ and $F_q$, the mounting locations should be as far from point M as possible, i.e., as near to the clamping plane as possible. However, it is important to consider the end effects of the clamping apparatus.

Secondly, in order to measure the vertical component of force, $F_p$, gages should be placed on the horizontal surface. These bending moments caused by $F_p$ result in the greatest longitudinal strains and, hence, highest measurement sensitivities. Similarly, gages for measuring the horizontal component of force, $F_q$, should be placed on the vertical planes, where longitudinal strains due to $F_q$ are maximum.

These fundamental considerations lead directly to a scheme for strain gage placement which will optimize measurement of $F_p$ and $F_q$. With reference to Figure 4a, we note that $F_p$, the vertical component of force can be most easily sensed by strain gages 1, 2, 5 and 6 located on the horizontal surface. The bridge arrangement of Figure 4, Bridge 1, shows how the strain gages form a four-arm bridge. Similarly, we note that $F_q$, the horizontal component of force can be best sensed by strain gages 3, 4, 7 and 8 located on the vertic 1 surface. The bridge arrangement of Figure 4b and 4c shows how these strain gages form a four-arm bridge. The Wheatstone bridge configurations shown in Figure 4 provide both maximum strain sensitivity and maximum thermal compensation.

Based on this strain gage placement scheme we can analyze the effect of the horizontal force, $F_q$ on the vertical force strain gages. If the gages are mounted symmetrically with respect to the vertical axis, bending moments due to $F_q$ cause a positive strain at gages 2 and 5 and a negative strain of equal magnitude at gages 1 and 6. This change in Bridge 1 causes no net output. This configuration allows Bridge 1 to measure strains caused by $F_p$ alone, while Bridge 2 will indicate only $F_q$. Crosstalk between $F_p$ and $F_q$ will be present only due to gage mounting inaccuracies.

The effect of the axial force on the horizontal and vertical force strain gages will be small since the magnitude of $F_r$ is small compared to $F_p$ and $F_q$ ($\sim$1/4) and since a and c (Figure 2b) are small compared to 1 ($\sim$1/3). Thus the resulting imbalance on bridges 1 and 2 due to $F_r$ will be small ($\sim$1/12) compared to the imbalance resulting from $F_p$ and $F_q$.

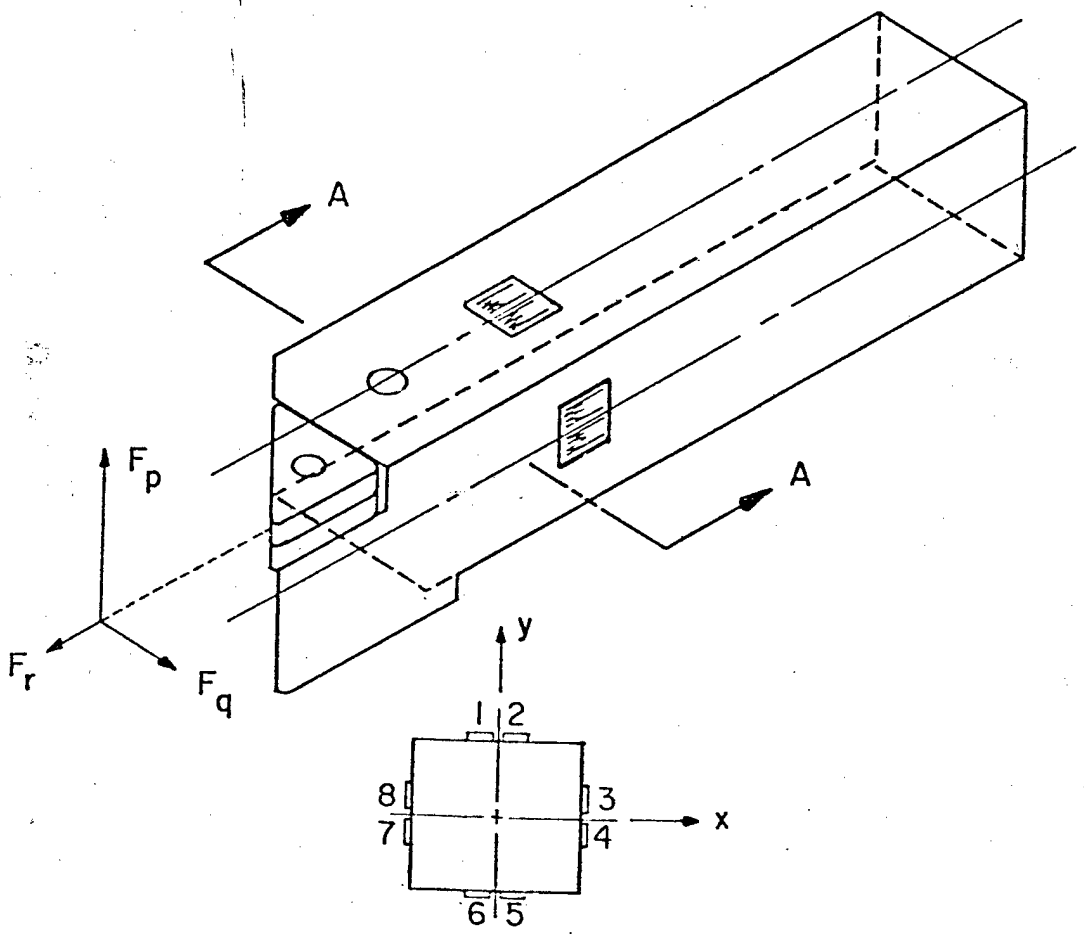


SECTION A-A

FIGURE 4a: STRAIN GAGE PLACEMENT FOR VERTICAL AND HORIZONTAL FORCE COMPONENT MEASUREMENT

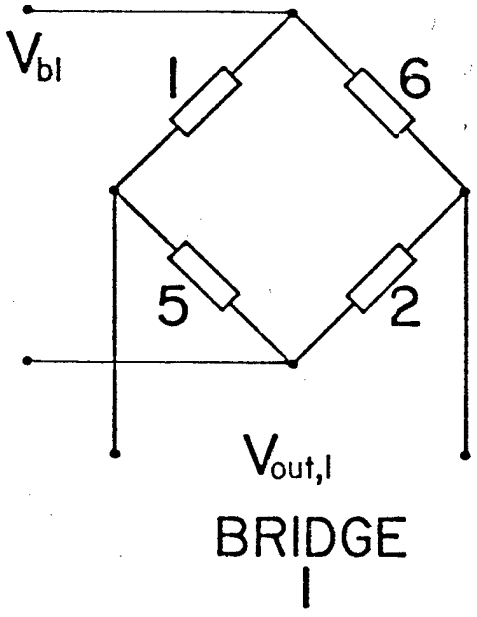


FIGURE 4b: BRIDGE ARRANGEMENT FOR VERTICAL FORCE, $F_p$

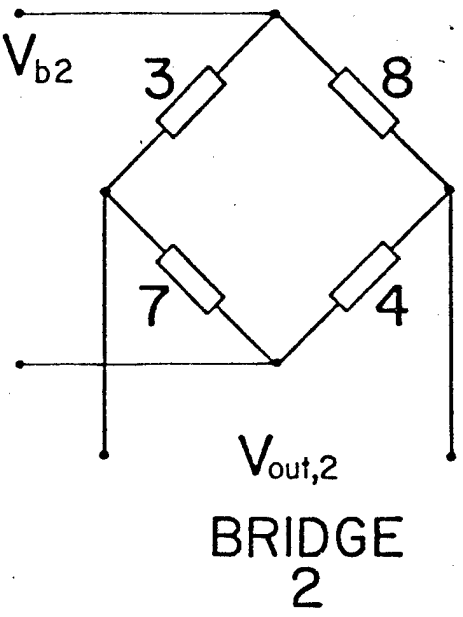


FIGURE 4c: BRIDGE ARRANGEMENT FOR HORIZONTAL FORCE, $F_q$

### 4.1.2 Axial Component, $F_r$

Next, consider the placement of gages to measure the radial force component, $F_r$. Because there is no mechanical advantage to amplify the radial strains, this signal is the smallest in magnitude. It is subject to influence from the two orthogonal forces $F_p$ and $F_q$ and therefore is the most difficult to measure. The question is thus raised: Where can strain gages be placed which will maximize sensitivity to $F_r$ and minimize the crosstalk from $F_p$ and $F_q$?

One obvious possibility for minimizing cross effects is to place gages near as possible to point M, thereby minimizing the moment arms for $F_p$ and $F_q$. However, near point M possibilities are greatest for physical contamination from metal chips and lubricating oil, high temperatures and impact damage. In addition, since lead wires must be run from the gages out of the toolholder, one axial location for gage placement would be advantageous. Therefore, given these considerations, where might gages be located a distance $l$ from the cutting point which would minimize effects of $F_p$ and $F_q$?

We know from simple analytical considerations that a plane exists along which the displacement due to bending moments induced by $F_p$ and $F_q$ is zero. Furthermore, it can be shown [1] that this plane is inclined on angle $\beta$ from the horizontal axis where

$$\tan \beta = \frac{F_q}{F_p} \quad . \qquad 4\text{-}1$$

Figure 5 illustrates this neutral plane location. From Eq. 4-1 we can see that the location of zero strain due to bending moments is a direct function of the ratio $F_q/F_p$. If a strain gage were located at the intersection of this neutral plane and a vertical surface (points $P_1$ and $P_2$), it would not be sensitive to strains induced by $F_p$ and $F_q$. Therefore, it could be used to measure compressive strain due to axial force $F_r$ alone.

Next, let us determine the location of Points $P_1$ and $P_2$. Eq. 4-1 shows us that we must know the force ratio $F_q/F_p$ if we are to locate these points. Fig. 6 shows a typical example of this force ratio as a function of tool wear. We can see that $(F_q/F_p)$ varies from about 0.4 to 0.5 over the range of tool wear illustrated. If we were to locate a strain gage at the position corresponding to $F_q/F_p = 0.5$, the effects on that gage due to $F_p$ and $F_q$ would diminish over tool life. So, as tool wear increased, our crosstalk effects would decrease by about 20% over the range of tool wear illustrated. Thus, the effectiveness of our matrix methods would increase as tool wear progresses. We conclude that the gages for measuring the axial force component should be located at points $P_1$ and $P_2$ where $\tan \beta \approx 0.5$.

Figure 7a-b illustrates the strain gage locations for sensitivity to $F_r$ which arise from the above considerations. In order to maximize system sensitivity and minimize error due to temperature effects, compl. four-arm bridges should be used. However, in the case of this radial component (a pure compressive load) a four-arm bridge of axial gages would yield zero output. Three options were considered for this measurement.

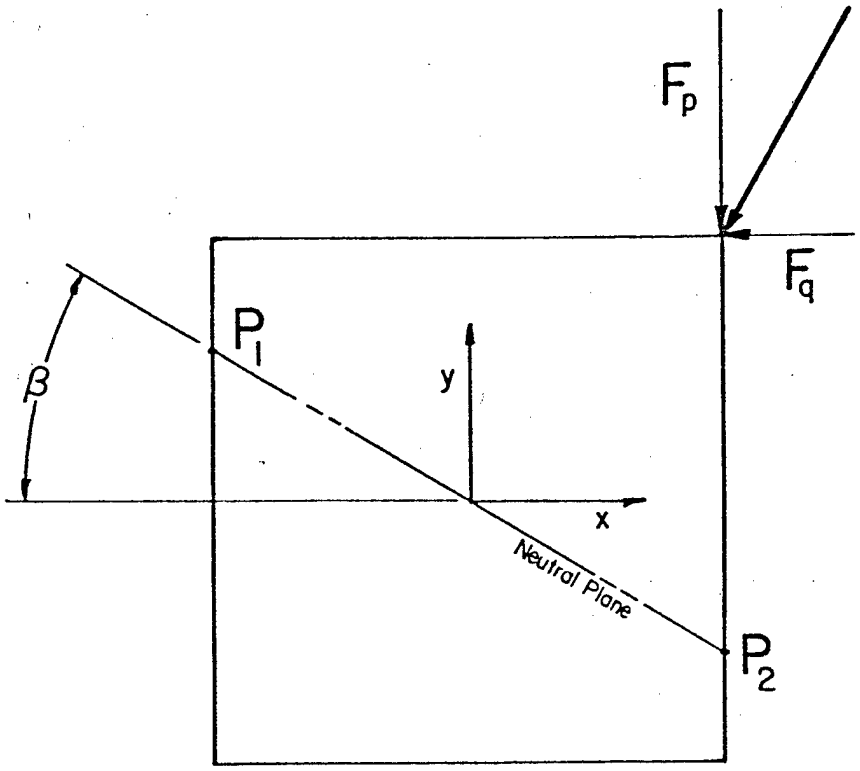


FIGURE 5: LOCATION OF NEUTRAL PLANE FOR UNEQUAL VERTICAL AND HORIZONTAL FORCE COMPONENTS

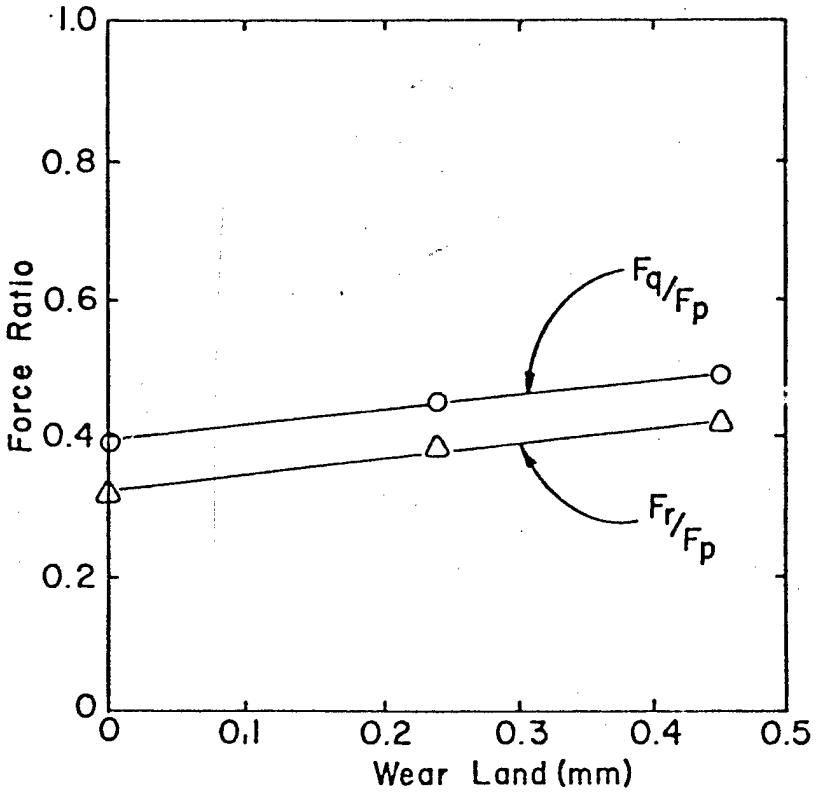


FIGURE 6: FORCE RATIO VERSUS WEAR LAND [2]

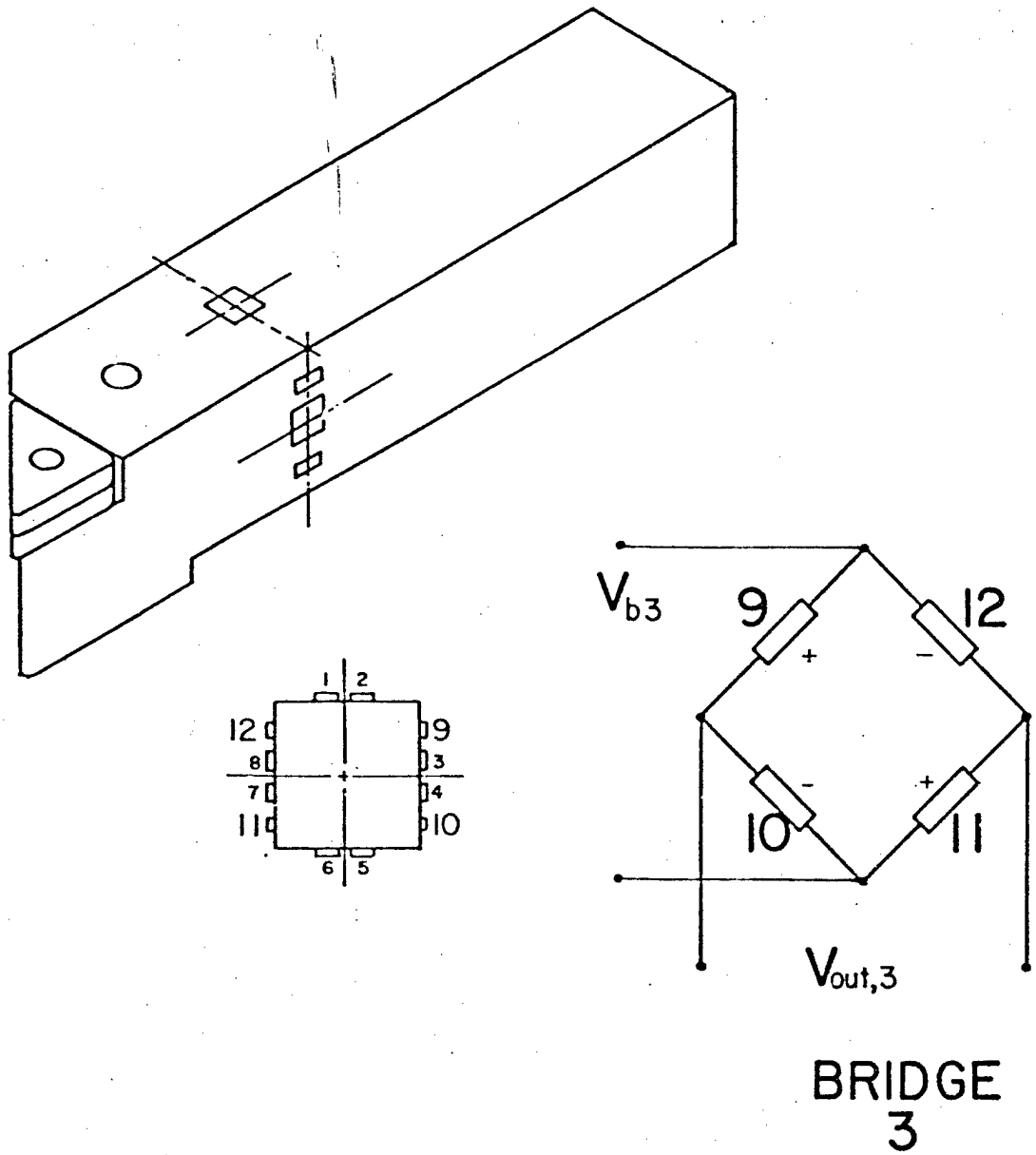


FIGURE 7a: STRAIN GAGE PLACEMENT FOR AXIAL FORCE COMPONENT MEASUREMENT CONFIGURATION A

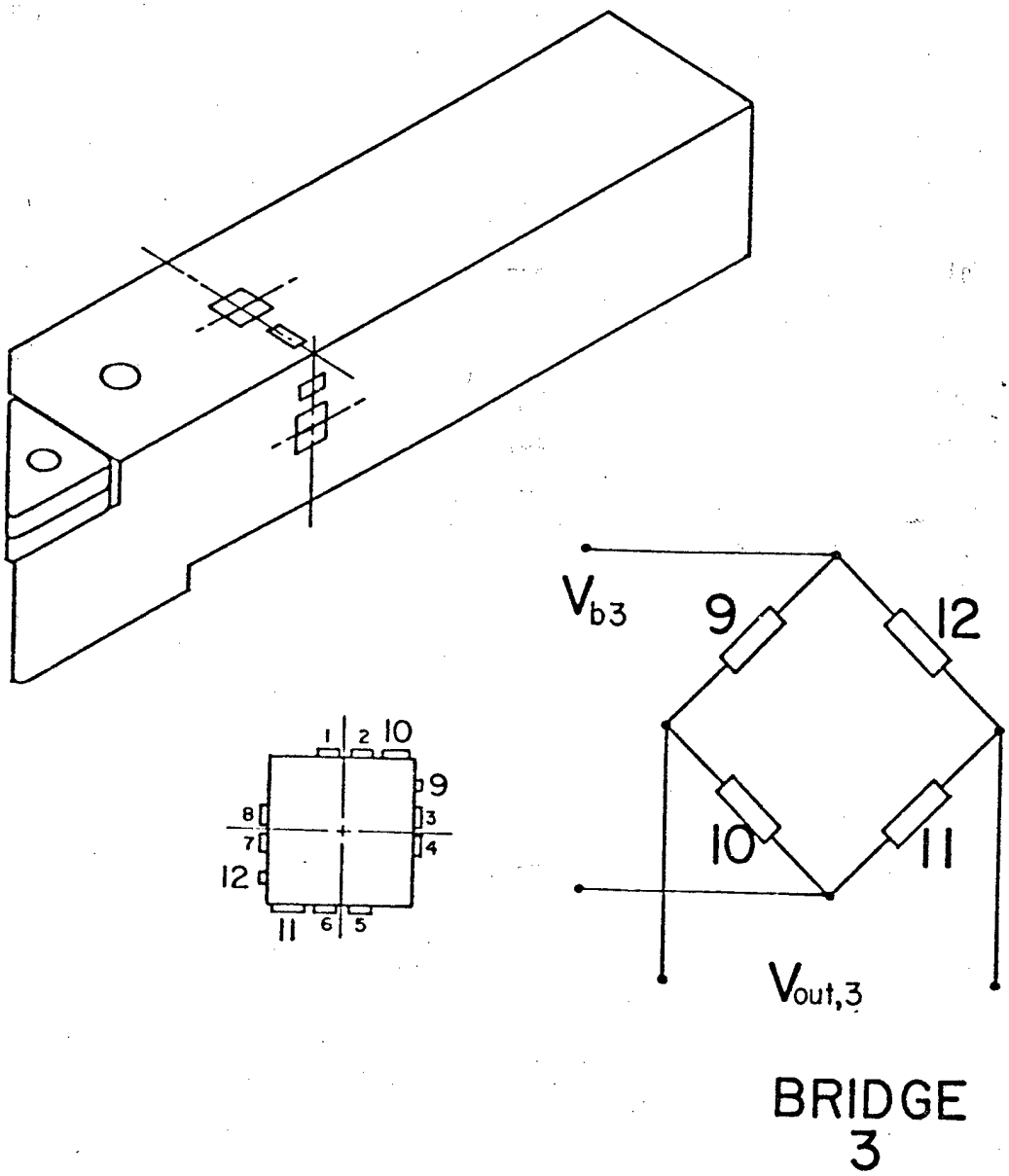


FIGURE 7b: STRAIN GAGE PLACEMENT
FOR AXIAL FORCE COMPONENT
MEASUREMENT CONFIGURATIONS B AND C

They are described below.

Configuration A

Four axial semiconductor gages, using two negative and two positive strain sensitivities (Fig. 7a). This configuration represents the highest potential strain sensitivity, since it allows the use of a full bridge with high strain sensitivity and potential temperature compensation. However, the peculiarities of semiconductor gage characteristics make this an unworkable solution. (Refer to Section 7.2 for a discussion of the problems encountered with this measurement scheme.)

Configuration B

Four N type semiconductor gages mounted on the toolholder with two located along and two located normal to the axis of the toolholder. See Figure 7b. This configuration yields slightly decreased sensitivity over a half-bridge configuration due to the added Poisson effect in the direction perpendicular to the longitudinal axis under compressive loading. In addition, this configuration allows bridge self-temperature compensation. The disadvantage of this configuration is the relatively high cost of semiconductor gages.

Configuration C

Four high resistance foil strain gages mounted in a configuration similar to B. That is, two gages mounted along the toolholder axis and two mounted normal to the toolholder axis. High

gain electronics are necessary to achieve the required sensitivities (approximate gain of 10,000).

## 4.2 Analytical Model

We have seen in Sec. 3.2 that, in general, the outputs of three randomly positioned strain gage bridges are sufficient to determine three orthogonal components of force. In addition, we can define a set of influence coefficients ($b_{ij}$) such that

$$\begin{bmatrix} F_p \\ F_q \\ F_r \end{bmatrix} = \begin{bmatrix} b_{11} & b_{12} & b_{13} \\ b_{21} & b_{22} & b_{23} \\ b_{31} & b_{32} & b_{33} \end{bmatrix} \cdot \begin{bmatrix} V_1 \\ V_2 \\ V_3 \end{bmatrix} \qquad 4\text{-}2$$

This equation shows that once the coefficents ($b_{ij}$) have been determined, a unique relationship has been defined relating force inputs to bridge outputs. This technique provides a simple method for measuring the three components of cutting force.

In Sec. 4.1 we found that one could identify strain gage positions which would make each bridge sensitive mainly to one force component and only minimally affected by the other two. That is, we can position the gages so that the diagonal terms of the B-matrix ($b_{11}$, $b_{22}$, $b_{33}$) are large in comparison to the off-diagonal terms. We have identified a series of gage positioning options to implement these techniques.

In this section we shall present a summary of the analytical model for predicting the values of ($b_{ij}$) given toolholder geometry and gage positions.

In the Appendix A the reader can find a detailed treatment of this model for one of the options of Sec. 4.1.2.

To begin with, we can model the toolholder of Fig. 2b as a cantilever beam clamped a distance L from the cutting point M. This beam is loaded at M by three orthogonal force components $F_p$, $F_q$ and $F_r$. We can then calculate the resulting twelve strains ($\varepsilon_1 - \varepsilon_{12}$) at each gage site. The result of this analysis is an expression relating each strain to the three force inputs which has the form

$$\varepsilon_n = a_{n_1} F_p = a_{n_2} F_q + a_{n_3} F_r. \qquad 4\text{-}3$$

We know that for small strains, the output of the Weatstone bridges of Sec. 4 can be expressed by a linear summation of each gage output. For example, for Bridge 1 of Fig. 4b, we can write

$$V_{out,\ 1} = F_{b_1}(S_1\varepsilon_1 + S_2\varepsilon_\delta - S_5\varepsilon_5 - S_6\varepsilon_6) \qquad 4\text{-}4$$

Where:

$V_{b_1}$ = bridge excitation voltage

$S_1$ = gage factor for gage 1, etc.

$\varepsilon_1$ = strain at gage site 1, etc.

By combining Eq. 4-3 and 4-4, we arrive at an expression which can be reduced to the form

$$V_1 = b'_{11}F_p + b'_{12}F_q = b'_{13}F_r \qquad 4\text{-}5$$

or, in matrix form

$$[V] = [B] [F] . \qquad 4\text{-}6$$

So, we see that Eq. 4-6 represents a unique linear relationship between three force inputs ($F_p$, $F_q$, $F_r$) and three bridge outputs ($V_1$, $V_2$, $V_3$). By premultiplying each side of Eq. 4-6 by $B^{-1}$, we find

$$[F] = [B]^{-1} [V] . \qquad 4\text{-}7$$

Eq. 4-7, then, is the expression identical to Eq. 4-2 which allows us to calculate unique values for $F_p$, $F_q$ and $F_r$ from $V_1$, $V_2$ and $V_3$ once the influence coefficients ($b_{ij}$) have been determined. Using these results, then, we can analytically predict transducer sensitivity from a stress analysis of a particular toolholder and gage geometry.

## 4.3 Results of Analytical Model

### 4.3.1 General Considerations

In the preceding section we outlined an analytical model for predicting transducer performance. This model was used to analyze trial configurations and to select proper strain gage materials. The model was implemented as a computer program to allow rapid analysis of various trial configurations. The complete FORTRAN listing of this coding may be found in Appendix B.

As we have seen in previous sections, the scheme for measuring vertical and horizontal force components was fairly straightforward. The configuration shown in Fig. 4 was used in all trial cases. The axial component measurement scheme was then varied to assess the performance of Configurations A, B

and C described in Sec. 4.1.2. The input parameters were transducer geometry, strain gage positioning, strain gage properties and signal conditioning parameters. The outputs of the program were strains at each gage site, and calculated influence coefficients ($b_{ij}$).

A summary of these calculations is presented in Table 1 for the three types of axial force measurement (the reader is referred to Appendix C for a complete tabulation of these results). The data shown are calcualted values for the influence coefficients introduced in Sec. 4.3. That is, these numbers represent the scaling factors for isolating one force component signal from the effects of the other two. Table 2 presents a reduction of these raw influence coefficients to values suitable for comparison to each other and for performance evaluation.

4.3.2. Vertical and Horizontal Force Components

Let us first consider the vertical and horizontal force component measurement. From Table 2 we can see that, in all cases, the sensitivity to force inputs is 20.9 V/lb. If we are to assume that random system noise can be limited to less than 10 mV, we find that inputs of 1 lb magnitude can be distinguished. Therefore, we can resolve forces on the order of 100 lb to within 1 lb. This accuracy is more than sufficient for normal machine tool applications.

4.3.3 Axial Force Component – Configuration A

We first reiterate that Configuration A consists of four semiconductor gages using two negative and two positive strain sensitivities. The results

$$\begin{bmatrix} F_p \\ F_q \\ F_r \end{bmatrix} = \begin{bmatrix} b_{11} & b_{12} & b_{13} \\ b_{21} & b_{22} & b_{23} \\ b_{31} & b_{32} & b_{33} \end{bmatrix} \begin{bmatrix} V_1 \\ V_2 \\ V_3 \end{bmatrix}$$

| Axial Configuration | Excitation Voltage | Gage Type | Gage Factor | Amplifier Gain (V/V) | Influence Coefficients Matrix - [B] | | |
|---|---|---|---|---|---|---|---|
| A | 3.5 | Semiconductor | 2-(+100)<br>2-(-100) | 1000 | -47.9 | 0 | 6.94 |
| | | | | | 0 | -47.9 | -8.27 |
| | | | | | 0 | 0 | -30.7 |
| B | 3.5 | Semiconductor | 4-(-100) | 1000 | -47.9 | 0 | 11.0 |
| | | | | | 0 | -47.9 | -13.1 |
| | | | | | 0 | 0 | -49.0 |
| C | 15 | Foil | 4-(2.0) | 10,000 | -47.9 | 0 | 9.57 |
| | | | | | 0 | -47.9 | -11.4 |
| | | | | | 0 | 0 | -42.5 |

Vertical and Horizontal Conditions: Four Foil Gages
Bridge Excitation Voltage = 5.0 V
Gage Factor = 2.0
Amplifier Gain = 2000 V/V

TABLE 1: RESULTS OF INFLUENCE MATRIX CALCULATION FOR TRANSDUCER CONFIGURATIONS A, B and C

Conditions

Force Input: 100 lb

| Gaging Configuration | | Sensitivity (mv/lb) | Physical Crosstalk before Influence Coefficients (%) | | |
|---|---|---|---|---|---|
| | | | Vertical | Horizontal | Axial |
| A | Vertical | 20.9 | -- | 0 | -14.5 |
| | Horizontal | 20.9 | 0 | -- | 17.3 |
| | Axial | 32.4 | 0 | 0 | -- |
| B | Vertical | 20.9 | -- | 0 | -23.0 |
| | Horizontal | 20.9 | 0 | -- | 27.3 |
| | Axial | 20.4 | 0 | 0 | -- |
| C | Vertical | 20.9 | -- | 0 | -20.0 |
| | Horizontal | 20.9 | 0 | -- | 23.8 |
| | Axial | 23.5 | 0 | 0 | -- |

TABLE 2: CALCULATION OF PHYSICAL CROSSTALK FOR THREE FORCE COMPONENTS, FOR INSTRUMENTED TOOL HOLDER CONFIGURATIONS A, B AND C

presented on Table 2 clearly show that Configuration A presents the best potential for sensitive axial force measurement. The sensitivity (32.4 mv/lb) is even greater than the vertical and axial cases. Furthermore, the physical crosstalk is the lowest of the cases analyzed (14.5-17.3%). So, if this configuration could be physically implemented, it would provide an excellent axial force measurement. However, it bears the disadvantage of the high cost of the four semiconductor strain gages.

### 4.3.4 Axial Force Component - Configuration B

Configuration B represents two axial and two perpendicular N type semiconductor strain gages mounted on the toolholder. It is another viable alternative for axial component measurement. In comparison to Configuration A, it shows both reduced sensitivity to force input and increased physical crosstalk. However, the sensitivity remains on the same order as the vertical and horizontal channels. The crosstalk, though high, remains in the acceptable range. That is, even if the error in implementing the influence coefficients were as high as 10%, the total error in indicated axial force would be no greater than about 3%. However, Configuration B shows no technical advantage over the configuration using standard foil strain gages. Since semiconductor gages are about five times as costly as foil gages, Configuration B would add about $30 to the manufacturing cost of the transducer while adding no increase in performance.

### 4.3.5 Axial Force Component - Configuration C

Configuration C is the same geometry as Configuration B but using high resistance foil gages. We can see from Table 2 that like Configuration B,

Configuration C offers decreased sensitivity and increased crosstalk in comparison with Configuration A. However, using the same arguments as in Configuration B above, we can see that the performance offered by Configuration C is fully acceptable for axial component measurement. In addition, this configuration minimizes the cost of strain gages and eliminates the extreme thermal sensitivity found in semiconductor gages. Therefore, Configuration C offers the more attractive alternative if Configuration A proves unworkable in practice.

### 4.3.6 Additional Observations from Analytical Results

We can draw a few other conclusions from the results of these analyses. First of all, we see that the use of conventional gain (1000-2000 V/V) electronics for axial force measurements would dictate the use of semiconductor strain gages with at least 3.5 VDC excitation voltage. In most cases, this value for excitation is within the region where thermal drift problems could be expected.

Secondly, in order to use conventional strain gages (GF ≈ 2.0) ultra high gain (10,000 V/V)amplification is required in conjunction with exceptionally high excitation voltage (≥ 15 VDC). This value for gain is higher than normally used since input noise ∿1μV can become significant. However, electronics of the quality required for this task is readily available at moderate cost.

In considering the effects of using excitation voltages greater than 15 VDC, one must again consider thermal drift problems. The power dissipated

by these strain gages can be written as

$$P = \frac{V^2}{R}$$

In order to operate within the limits recommended by strain gage manufacturers, power dissipation must be kept below 0.04W per gage. This results in

$$R = \frac{V^2}{P} = \frac{15^2}{.04} = 5625\ \Omega$$

So, we must use ultra-high resistance strain gages in order to realize proper sensitivity. Again, though not commonplace, such gaging material is presently commercially available at moderate cost.

### 4.3.7 Conclusions from Analytical Results

From the considerations above we can draw the following conclusions:

1. The suggested scheme for measuring horizontal and axial components should result in satisfactory transducer performance.
2. The Transducer Configuration A for measurement of axial force offers the highest potential transducer sensitivity at the expense of higher transducer manufacturing cost and higher susceptibility to thermal drift.
3. Transducer Configuration C offers a fully acceptable axial component measurement scheme while reducing transducer cost and thermal problems. However, such a method would require the use of more sophisticated high-gain signal conditioning and infrequently-used strain gage materials. If these difficulties can be overcome, Configuration C would be the best overall solution to the axial force measurement problem.

## 4.4 Cost/Benefit Considerations

The first research objective of this Phase I development program was to instrument a toolholder within the constraints of reasonable cost and utility. Based on the work conducted in this feasibility program, it is anticipated that a ruggedized production instrumented toolholder would be fabricated by placing a custom designed strain element at only four locations on a modified production toolholder. The estimated manufacturing cost of such a device would be approximately $100 in small quantities. Since such a device would be used continuously for several weeks before replacement, it would seem that the goal of reasonable cost has been obtained. Since custom strain elements can be ordered in quantity from present suppliers of strain gage rosettes, it would also appear that the instrumented toolholder could be reduced to a readily producible commodity.

The approach of utilizing custom designed strain elements will give the added benefit of allowing the location of one strain gage relative to another to be held very accurately. Therefore the time required to mount the gages accurately will be greatly reduced as only four elements will need to be located on the toolholder.

Matrix methods give an additional benefit in that any strain element alignment errors can be factored out by the matrix method. While it is desirable to locate the strain elements accurately for minimum crosstalk, matrix methods will reduce the requirement for gage placement accuracy and therefore help in making the toolholder a readily producible inexpensive product.

# 5. TRANSDUCER CONSTRUCTION

## 5.1 Description of Transducer Construction

The implementation of the foregoing transducer design involved mounting strain gages on a standard toolholder available for machines in use at AMTI. An aloris ADS 5-3 toolholder with 5/8 in square shank was modified to receive the necessary gages. Figure 8 shows a photographic view of this construction. Four surfaces were ground flat for gage mounting. A hole (.125 in) was drilled along the axis of the toolholder large enough to allow extraction of all lead wires for the strain gage bridges. At each gage mounting surface a smaller hole (.094 in) was drilled intersecting with the axial passage to lead wiring away from the gage sites. After mounting, the gages were covered with protective foam padding and aluminum foil tape for shielding. The wiring was carried from the transducer to the signal conditioners using shielded multi-conductor cable. Fig. 9 shows a photographic view of this construction.

### 5.1.1 Configuration A

The first prototype constructed used standard foil-type strain gages (120 Ω, GF = 2.015, thermally compensated to steel) for positions 1-8 in Fig. 7a. Positions 9-12, those sensitive to axial loading, used semiconductor gages (120 Ω, GF = ±100). Two of these were P-type doping (positive $\Delta R/R$ for positive $\Delta L/L$) and two were negative doping (negative $\Delta R/R$ for positive $\Delta L/L$). As described in Section 4.1, this configuration allowed measurement of a pure compressive load while retaining full bridge sensitivity. As described in Sec. 7.2, this configuration proved to have no thermal stability.

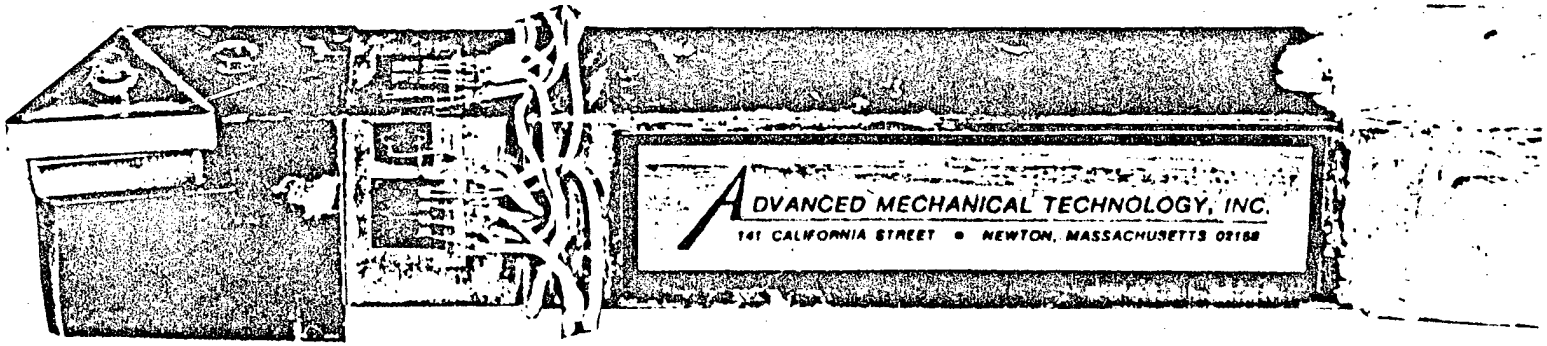


FIGURE 8: PROTOTYPE INSTRUMENTED TOOLHOLDER TRANSDUCER

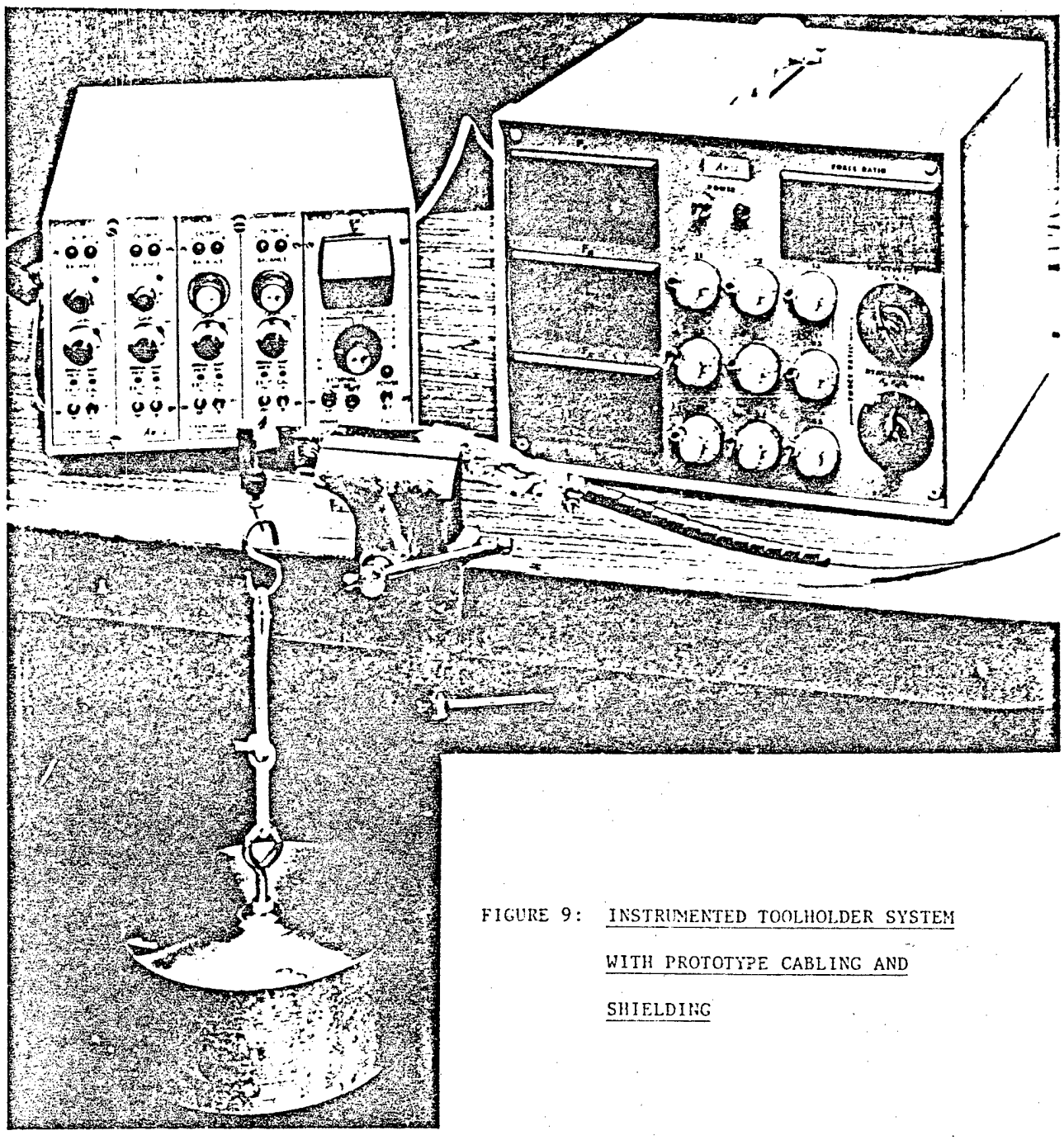

FIGURE 9: INSTRUMENTED TOOLHOLDER SYSTEM WITH PROTOTYPE CABLING AND SHIELDING

### 5.1.2 Configuration B

The second configuration used four N-type semiconductor gages (120 Ω, GF = -100, thermally compensated for steel) with two mounted perpendicular to the shank axis. This configuration permitted greater thermal stability at the expense of reduced bridge sensitivity. This configuration is pictured in Fig. 10.

### 5.1.3 Configuration C

Due to limitations of time and capital, Configuration C was not tested in a transducer prototype. However, a series of tests were performed to establish the viability of this configuration. The reader is referred to Sec. 7.3.3 for a summary of these brief tests.

## 5.2 Conclusions from Transducer Construction

This prototype demonstrates all the desired features for a satisfactory production-oriented dynamometer. It uses a standard toolholder and mounts in a standard tool post. As will be shown in later sections, it can produce accuracy and utility comparable to a research lathe dynamometer. Finally, it can be constructed for a cost low enough to permit widespread application in conventional and numeric-controlled machining operations.

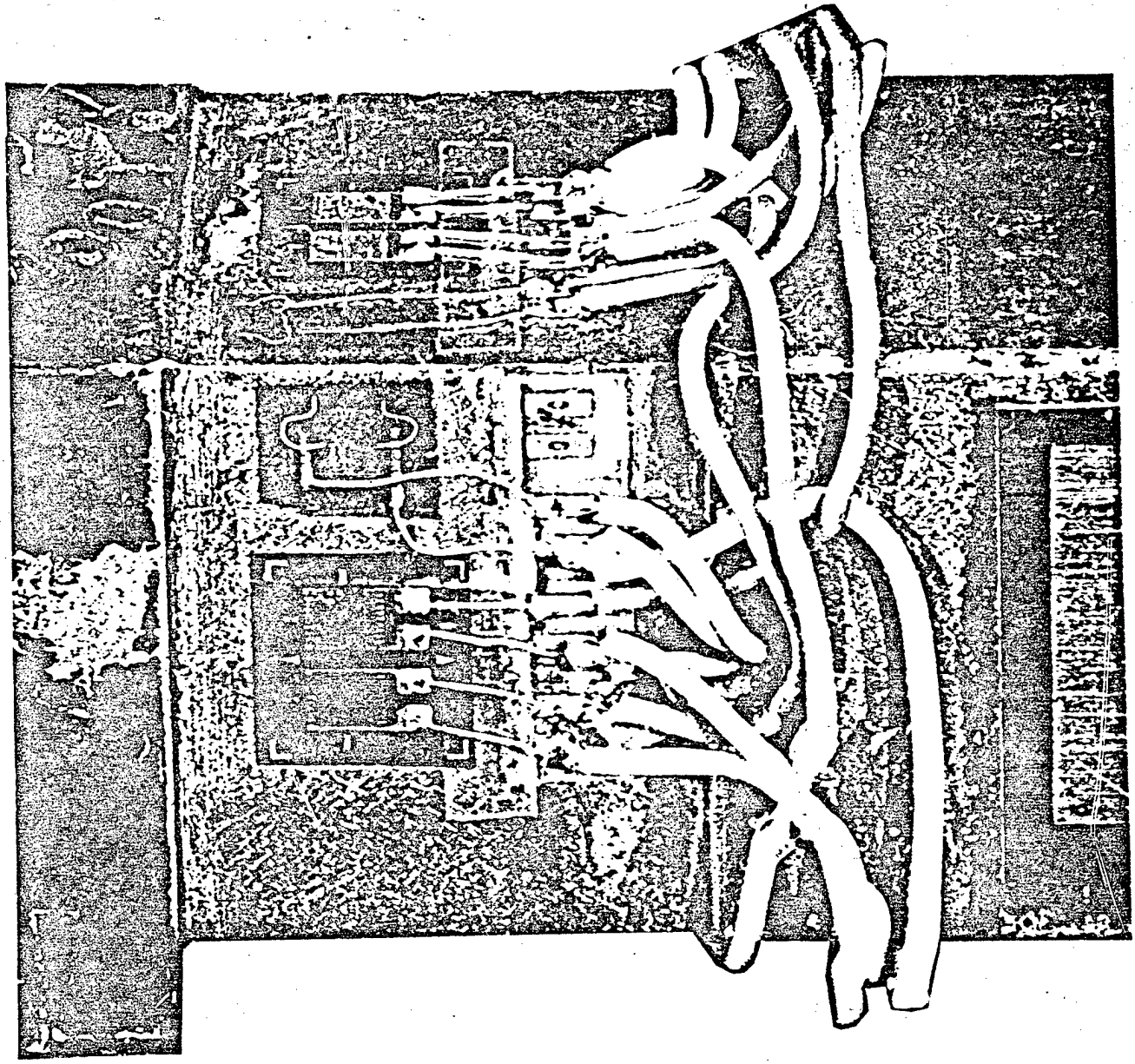

FIGURE 10: INSTRUMENTED TOOLHOLDER GAGE PLACEMENT SHOWING AXIAL CONFIGURATION B

# 6. PROTOTYPE SYSTEM SIGNAL CONDITIONING AND PROCESSING

The general requirements for signal conditioning and processing can be summarized in graphic form by Fig. 11. Low-level strain gage signals must be amplified to useable voltage levels. These three signals must then be manipulated to perform the multiplication by the influence coefficients. Finally, the results must be displayed or recorded as force components with engineering units (lb, kg).

In this prototype system, bridge exictation and amplification was performed by standard strain gage signal conditioners (Vishay 2120A). This equipment provided suitable excitation and gain for all transducer testing.

The matrix manipulation was performed by an analog circuit built for this program. It represented the simplest and most straightforward means of inputing coefficients and displaying results. Even though this function could have been performed using a computer system, the analog circuit presented a solution with the simpler implementation and debugging requirements.

Fig. 12 presents a block diagram of one channel of the analog circuitry. (The detailed electronic circuit diagram is presented in Appendix C.) Influence coefficients ($b_{ij}$) were input using precision 10-turn potentiometers with graduated dials. The resulting signals were summed using a standard op-amp inverting-summer-circuit. The force signals were displayed on digital panel meters in engineering units (lbf). An analog dividing circuit allowed display of force ratios. Finally, any recording was done with a multichannel strip chart recorder.

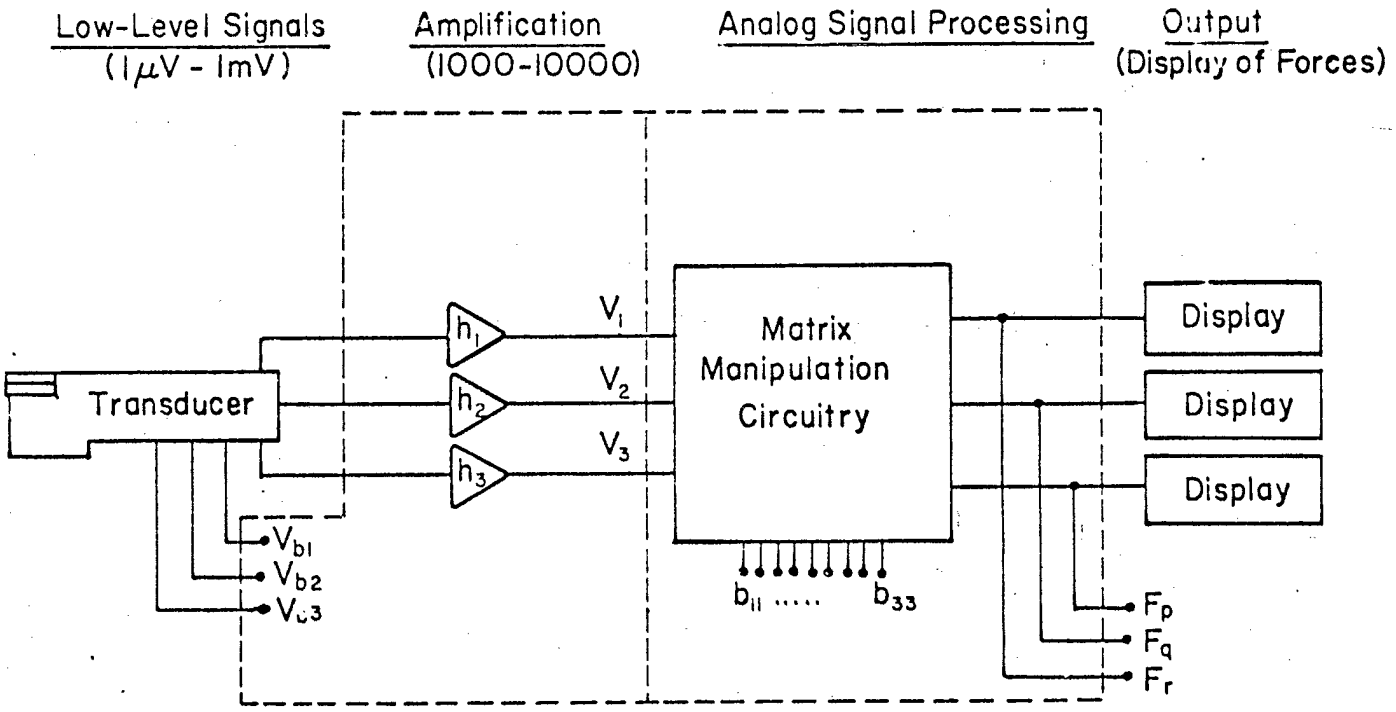


FIGURE 11: SIGNAL CONDITIONING AND PROCESSING REQUIREMENTS

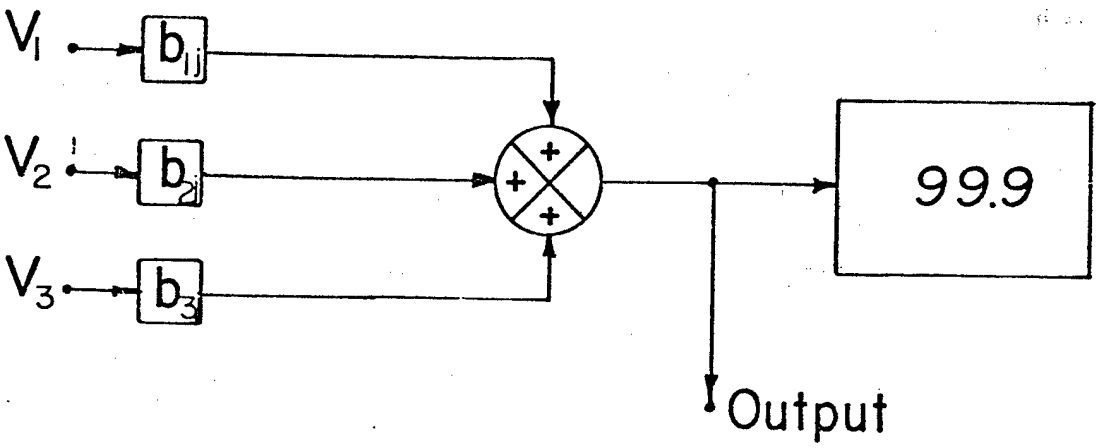


FIGURE 12: BLOCK DIAGRAM OF ANALOG MATRIX MANIPULATION FOR SIGNAL PROCESSING

Fig. 13 shows the prototype signal processing system. This analog circuitry performed its function in a satisfactory way. The system maintained accuracies within ±1% of full scale indications. Transducer calibrations were performed using the same voltage indication as used for force display. Therefore, any system errors were eliminated in the system calibration technique. A production circuit of similar design would operate well if the intended system function were force and force ratio display alone.

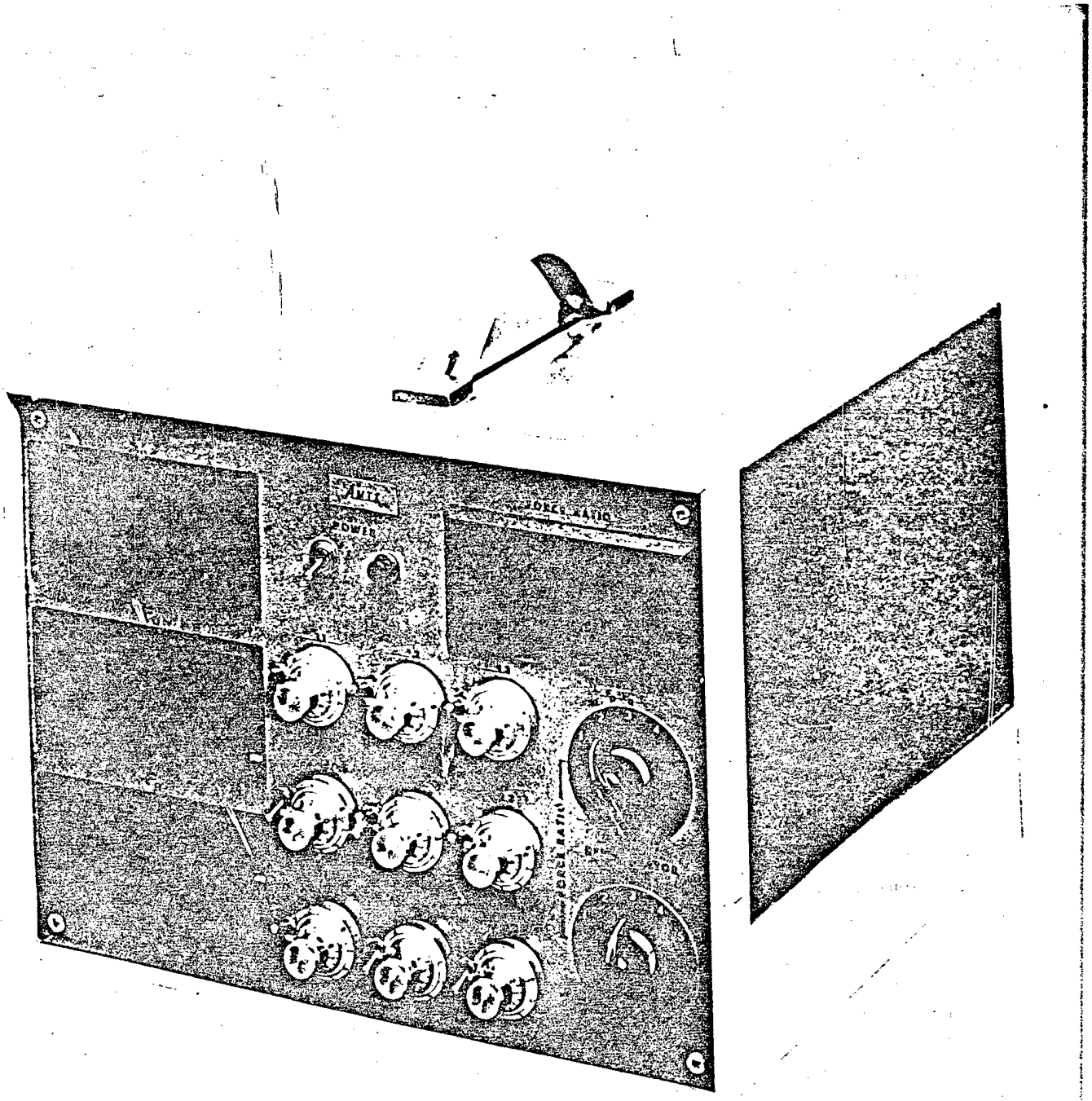

FIGURE 13: PROTOTYPE ANALOG SIGNAL PROCESSING SYSTEM

# 7. TRANSDUCER TESTING RESULTS

The transducer prototype was tested using three separate techniques. These included:

a. Static calibration and testing

b. Measurement of dynamic output during actual machining operations

c. Comparison with a research lathe dynamometer during machining operations.

The first of these techniques was used to determine quantitative performance by measuring sensitivity, linearity and stability. The second and third techniques were employed to give a qualitative view of transducer performance and not to study specific dynamic characteristics.

## 7.1 Static Calibration Procedure

In order to determine the values for the influence coefficients for the actual transducer, a static calibration technique was used. Weights hanging from flexible connections were used to apply the horizontal, vertical and axial forces. A test fixture was constructed which simulated the application of cutting forces at a cutting point. This fixture is shown in Fig. 14. It was constructed so that three tapped holes aligned in the horizontal, vertical and axial directions passed through a single point. When attached to the toolholder, this point coincided with the top of the cutting tool.

The toolholder was then mounted in a secure position and leveled in the proper orientation, as pictured in Fig. 15. A known weight was hung

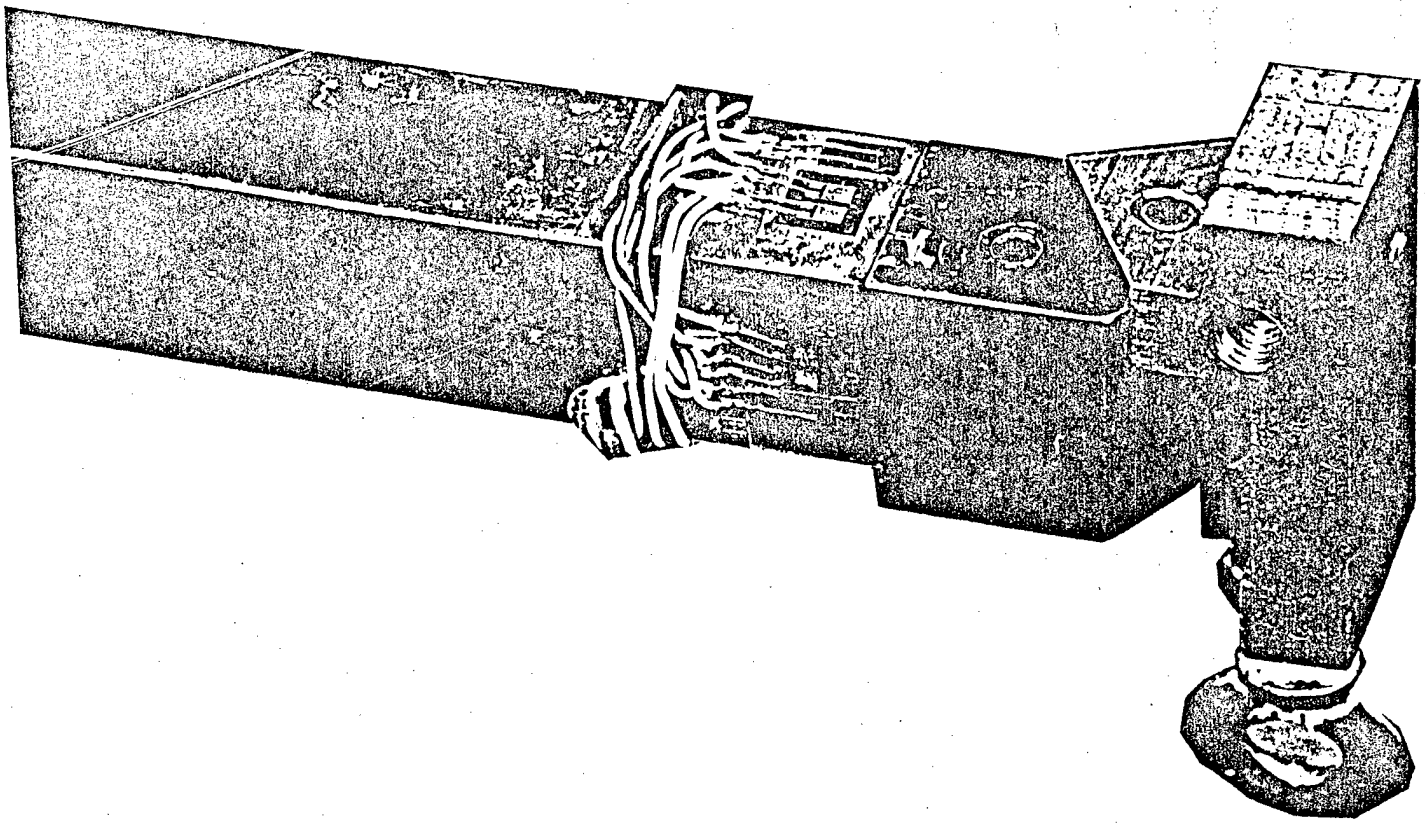

FIGURE 14: INSTRUMENTED TOOLHOLDER WITH STATIC CALIBRATION FIXTURE INSTALLED

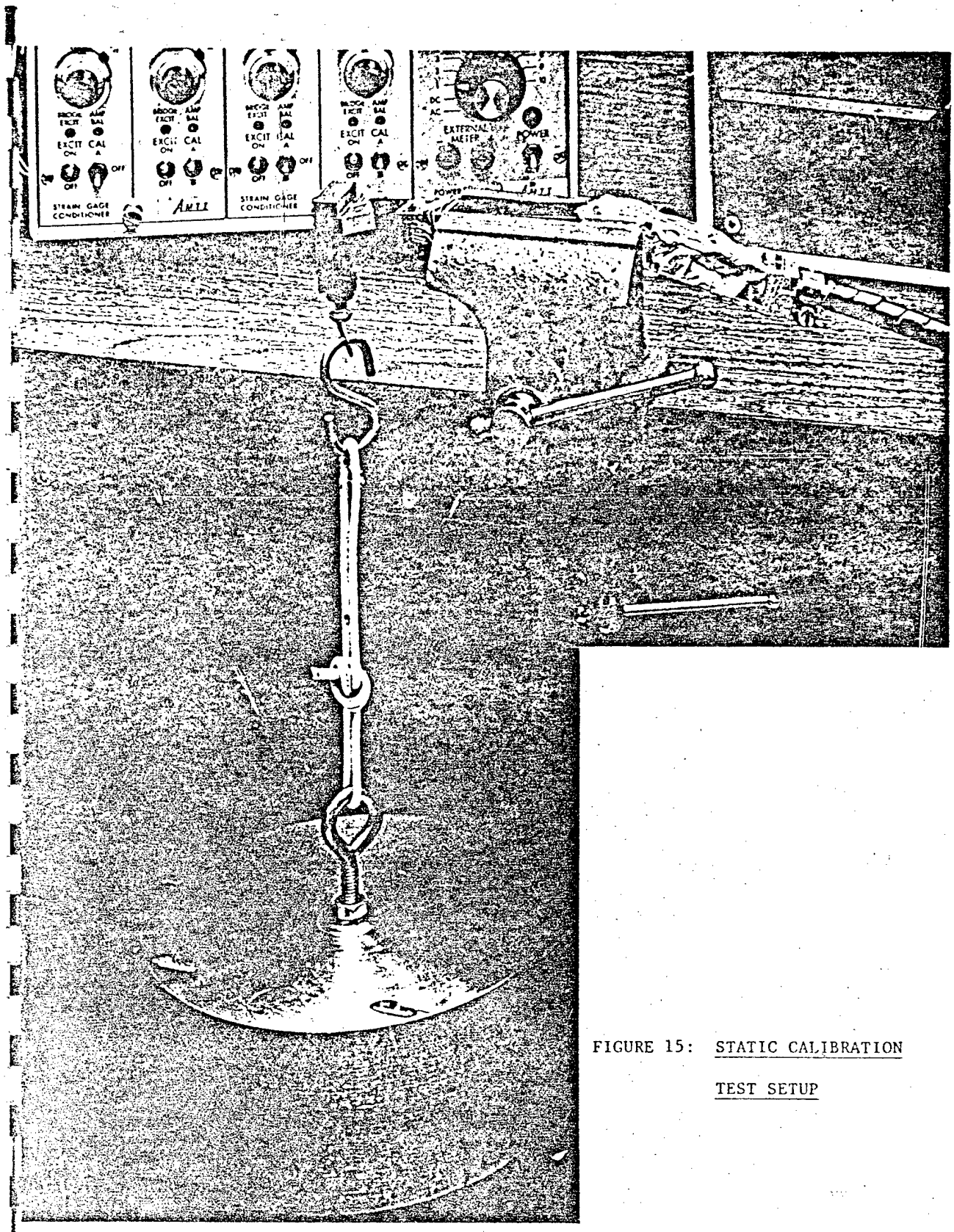


FIGURE 15: STATIC CALIBRATION TEST SETUP

from an eyelet screwed into the proper fixture hole. The application of this test weight resulted in outputs from the three bridges, measured using the signal processing "black box". The outputs were recorded and the procedure repeated for the other two directions.

This procedure generated a set of nine numbers which related three force inputs to three bridge outputs. By dividing these recorded values by the measured weight of the test weight, a set of numbers resulted which corresponded to the $B_{ij}$ values in the equation.

$$\begin{bmatrix} F_p \\ F_q \\ F_r \end{bmatrix} = \begin{bmatrix} b_{11} & b_{12} & b_{13} \\ b_{21} & b_{22} & b_{23} \\ b_{31} & b_{32} & b_{33} \end{bmatrix} \begin{bmatrix} V_1 \\ V_2 \\ V_3 \end{bmatrix}$$

Using a programmable calculator, we can invert the B matrix and arrive at the set of influence coefficients described in Equation 4.4. These coefficients were then set on the appropriate potentiometers of the Analog Signal Processing System shown in Figure 14. Values were checked for accuracy by recalibrating with the dead weights and observing the resultant forces displayed on the signal processer.

This procedure proved to be adequate for these testing purposes. In addition, it promises to be an excellent, easily performed calibration procedure for production transducers.

## 7.2 Measured Performance during Static Testing

Table 3 and Fig. 16 show the results of static testing performed on the instrumented toolholder prototype using Configuration B of Sec. 4.1.2.

| | Vertical | Horizontal | Axial |
|---|---|---|---|
| Sensitivity (mV/lb) | 19.4 | 19.6 | 35.2 |
| Linearity (% FS) | 1.2 | 1.2 | 3.7 |
| Drift (mV, RTO) | 0 | 0 | 20 max |
| Excitation Voltage (V) | 5 | 5 | 3.5 |
| Gain (V/V) | 2000 | 2000 | 1000 |
| Strain Gage Type | Foil | Foil | Semiconductor |
| Gage Factor | 2.01 | 2.01 | 100 |

TABLE 3: MEASURED PERFORMANCE - STATIC TESTING

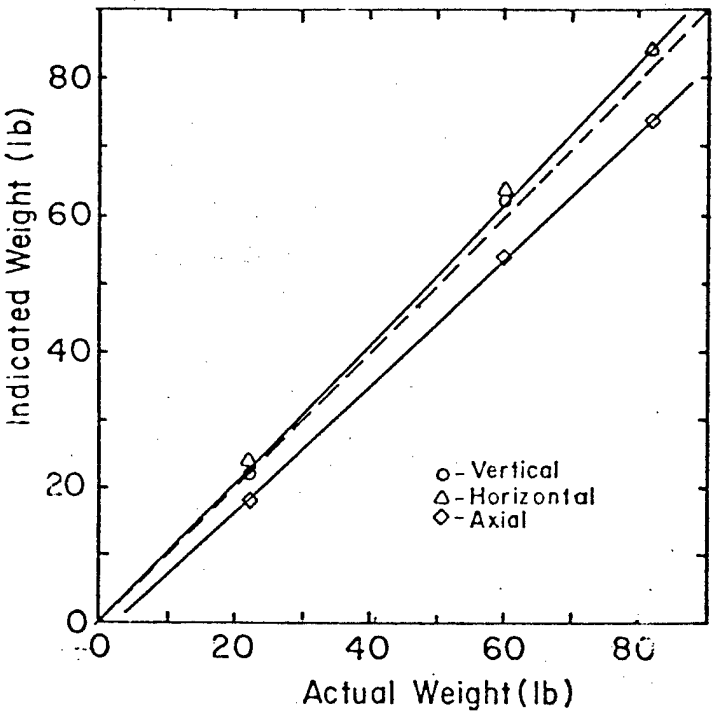


FIGURE 16: RESULTS OF STATIC CALIBRATION TESTING

The determination of influence coefficients was performed with three different calibration weights (22, 60, 82 lb). Since the weight could be read only to the nearest pound, suitable accuracy could be obtained only using the highest weight (82 lb). Tests performed at lower weights confirmed the inaccuracies expected from display uncertainties.

The data plotted on Fig. 16 shows the linearity and zero shift of the instrument. As expected, the vertical and horizontal channels showed acceptable linearity and stability. However, the axial channel constructed with semiconductor gages revealed a lack of linearity and thermal stability even when long settling times were allowed. These results are compatible with all other qualitative observations of this semiconductor strain gage application.

## 7.3 Discussion of Results of Static Testing

### 7.3.1 Configuration A

The major technical problem encountered in this program involved the linearity and stability of the axial force component due to the semi-conductor strain gage bridge. The first prototype constructed used two P-type (positive gage factor) and two N-type (negative gage factor) semiconductor strain gages as shown in Fig 7a. This arrangement provided excellent strain sensitivity. However, as alluded to in a previous section, this arrangement showed poor thermal stability. A brief look at the characteristics of semiconductor strain gages will reveal the reasons for this thermal drift.

Fig. 17 shows the relationships for gage factor and temperature coefficient of resistance versus temperature for P-type and N-type dopings.

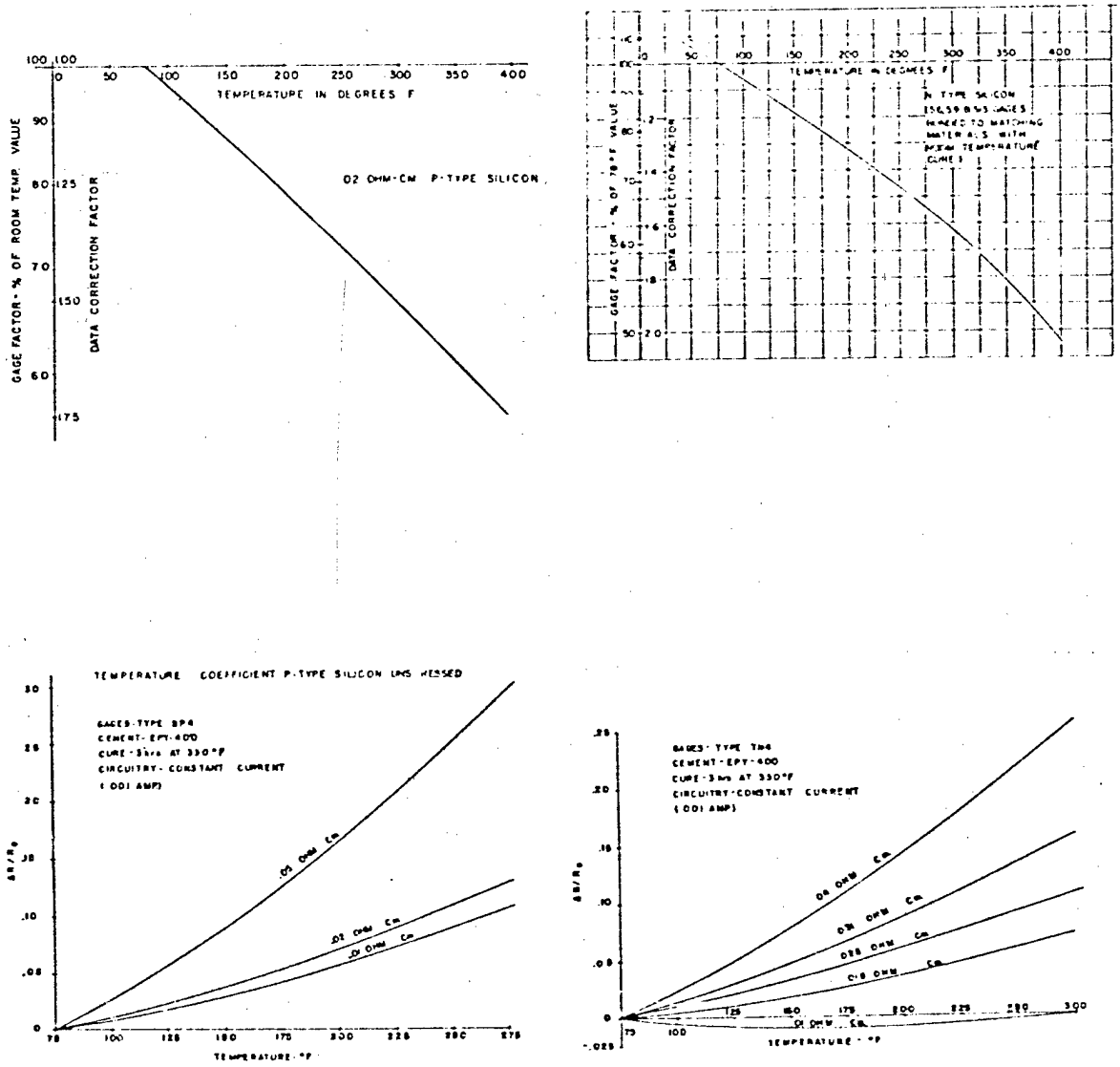


FIGURE 17: VARIATION OF GAGE FACTOR AND TEMPERATURE COEFFICIENT WITH TEMPERATURE FOR SEMICONDUCTOR STRAIN GAGE MATERIALS [5].

As is apparent, these vary significantly over small temperature changes. So, for a small temperature change the N-type and P-type gages will change differently, resulting in a bridge unbalance and large apparent strain. In addition, P-type characteristics do not allow these gages to be self-compensated to particular materials (In the case of N-type gages, doping characteristics permit self-temperature-compensation.). Thus, P-type and N-type gages cannot be used in the same bridge where any even miniscule temperature variations occur.

### 7.3.2 Configuration B

The second gage configuration, seen in Fig 7b, employed four N-type self-compensated strain gages. Two were mounted in the axial direction and two were mounted perpendicular to the axis to provide further bridge temperature compensation. As an initial check of thermal stability, this bridge was excited and the output recorded over a period of time. It was found that, as the room temperature changed by about 12°F, the bridge became unbalanced by roughly 100 mV. With a bridge sensitivity of 32 mv/lb, the net thermal error in terms of force was .25lb/°F. Thus for the large temperature excursions expected in machining operations (~100°F), we should expect thermal errors on the order of the total force indication (25 lb). Since self-compensated gages and a self-compensated bridge configuration were used, it is not apparent what caused such large thermal drift. A possible source is dissimilar bonding conditions for each gage. However, the net effect of the errors was to produce an unacceptable axial component measurement.

### 7.3.3 Configuration C

The limits of time and capital did not allow the construction of a prototype of Configuration C. However, in order to investigate the feasibility of using high-resistance strain gages at excitation voltages, a simple test piece was constructed. Several different bridge configurations were mounted on a 1 x 1-1/8 in block of steel. Weights were hung in a fashion identical to techniques described in Sec. 7.1. As expected, the bridges yielded outputs linear with weight. The output showed reasonable stability with 15 VDC excitation voltage applied to gages with 5KΩ nominal impedance. However, the feasibility of this strategy in an actual transducer must be determined in a later phase of work.

## 7.4 Measurement of Forces in Turning Operations

The prototype instrumented toolholder was tested in two separate turning operations: in a standard lathe at AMTI and in parallel measurements with a Cook research lathe dynamometer in the Materials Processing Laboratory at the Massachusetts Institute of Technology. Both sets of tests were intended to provide verification of the functionality of the transducer, not to provide a detailed study of the instrument's dynamic characteristics. In all of these tests the axial force channel was not used, since excessive thermal drift obscured the signal and introduced significant error into the other two channels. Figs. 18-20 provide two-channel traces recorded by strip chart in a number of cutting conditions. The instrument provided voltage outputs relatively free from extraneous electrical noise. In the AMTI tests, both vertical and horizontal channels showed good zero stability even in high-load, high-heat generation cases.

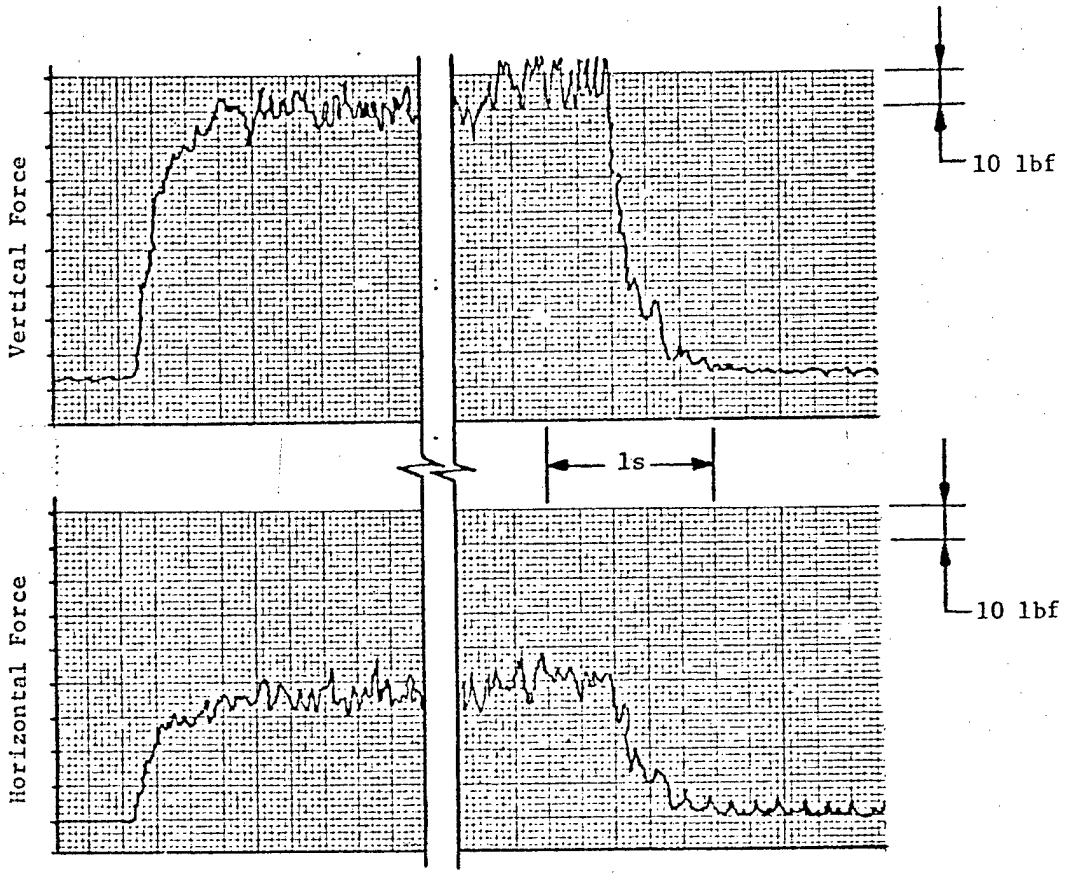


Conditions:

Material: Carbon Steel

Feed Rate: 0.68 ft/min

Depth of Cut: 0.030 in

Workpiece Surface Speed: 314 ft/min

(Traces accentuated for clarity)

FIGURE 18: RECORDED OUTPUT OF VERTICAL AND HORIZONTAL CHANNELS DURING LATHE OPERATION AT AMTI

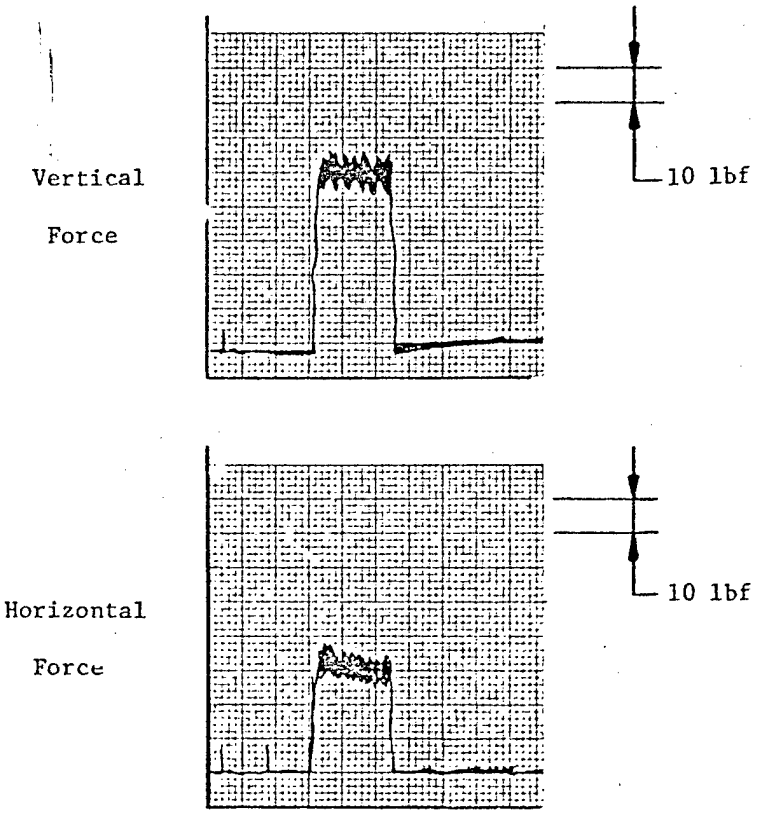


Conditions:

Material: Carbon Steel

Feed Rate: 0.34 ft/min

Depth of Cut: 0.040 in

Workpiece Surface Speed: 31[illegible] ft/min

FIGURE 19: RECORDED OUTPUT OF VERTICAL AND HORIZONTAL CHANNELS DURING LATHE OPERATION AT AMTI

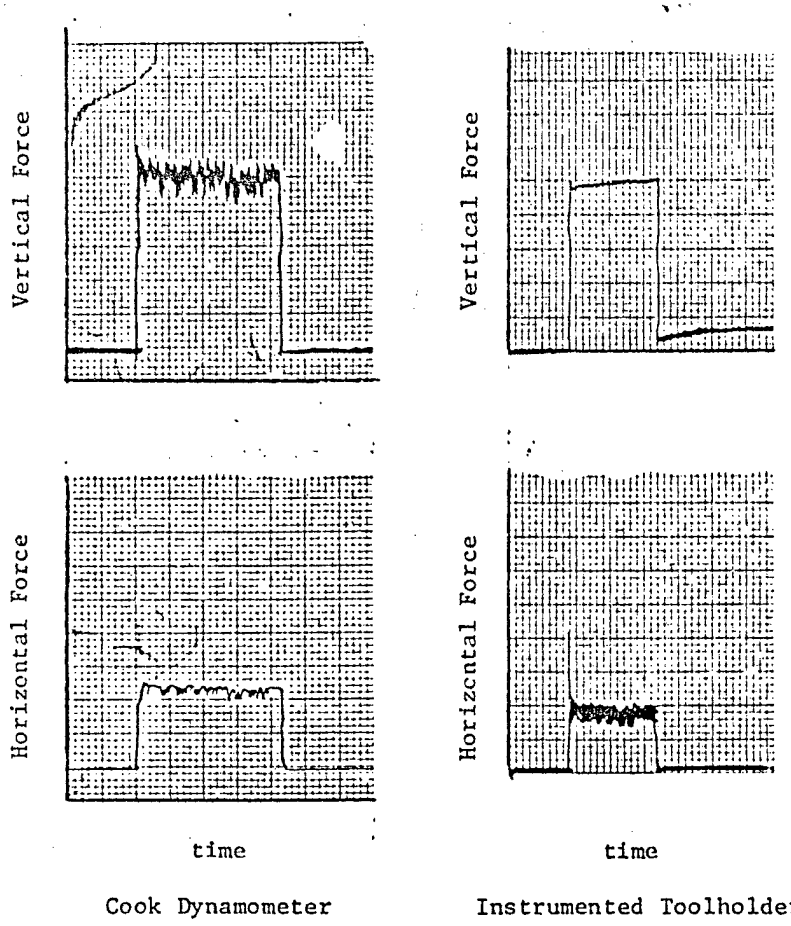


Conditions:

Material: Carbon Steel

Feed Rate: 0.21 ft/min

Depth of Cut: 0.026 in

Workpiece Surface Speed: 700 ft/min

(Traces accentuated for clarity)

FIGURE 20: COMPARISON OF TWO CHANNEL OUTPUTS OF INSTRUMENTED TOOLHOLDER AND COOK DYNAMOMETER DURING LATHE OPERATION AT MIT

The MIT tests shown in Fig. 20 were performed by making a similar cut (holding surface speed, horizontal fled and depth-of-cut) on the same stock in two different situations: one with the instrumented toolholder mounted in a standard tool post; one with an identical toolholder mounted in a research lathe dynamometer. As Fig. 20 shows, the two outputs reveal similar frequency characteristics and force levels. In addition, the force ratio $F_q/F_p$, a characteristic tool wear parameter, is roughly the same for the two cases. So, without regarding the detailed traces, the tests show that the instrument provides vertical and horizontal force indication with clarity and accuracy comparable to a research dynamometer.

## 8. ADVANCED SIGNAL PROCESSING

In general, the Instrumented Toolholder System generates three signals from three strain gage bridges. The external system must perform several operations on them in order to generate system outputs which indicate three force components. These functions include

a. amplifying signals to useful levels
b. multiplying signals by the influence coefficients and summing products in order to obtain force indication
c. generating an output necessary for direct or indirect observation of cutting forces.

These functions are common to any Instrumented Toolholder application. At this point several system options can be identified in order to provide input to a range of applications. At least three system options are apparent at the present time. These include:

a. a stand-alone analog signal processing system which provides an operator with force indication and tool wear/failure indication
b. a stand-alone microprocessor-based system which provides more sophisticated functions for an individual operator. These functions would be determined in a later research phase.
c. A subsystem which would provide signal input to a microprocessor-based computer-numeric-control (CNC) system.

Let us now consider these three options in more detail. Option (a) is the simplest, least expensive and least flexible of the options. Such

a stand-alone "black-box" would allow force transducer retrofit to any lathe able to hold a standard toolholder. The output of this system would permit inexpensive cutting force experimentation in a small machine shop or academic community. In addition, significant research (2)(3) has shown that simple functions of cutting forces can provide an indication of tool wear and possibly prediction of tool failure. Thus, with this inexpensive device, an operator can constantly be aware of the state of his cutting tool and his margin of safety to tool failure.

The design of this system option would be very similar to the simple signal processor used for this Phase I program. It would not differ significantly from the system diagram pictured in Fig. 11. Its function would remain the same, i.e., to display the force components derived from the three transducer signals.

Option (b) provides the next level of sophistication and capability to the retrofit user. Such microprocessor capability would afford the user variable tool condition criteria for different machining environments. Such a general-purpose system would be interchangeable from machine to machine, using the same electronic package to service a variety of transducers. Though a microprocessor-based system seems more complicated and perhaps more expensive, the wide variety of electronic components available today at low cost could make the market price extremely competitive with the analog-only system. Option (b) provides an attractive application for the emerging series of "analog microprocessors".

Option (c) extends the application of the ITH into the expanding field of CNC machining. As referenced above, research efforts have shown that low-cost cutting force component measurement provides one of the most promising schemes for monitoring tool wear, tool failure prediction and even optimization of cutting processes (4). The ITH provides such a low-cost force measurement technique which is readily interfaced to any computer-based numerical control system. This system is a straight-forward application of current data acquisition techniques which present no particular implementation difficulties. The frequency characteristics and response speed of machine tool operations (~100 Hz) present no problem to standard data acquisition circuitry. In fact, toolholder vibrations (~5-15 KHz) can be tracked with standard high-speed data acquisition techniques. In short, there are no foreseen barriers to the implementation of option (c) given standard, off-the-shelf microprocessor components.

The design of options (b) and (c) would be very similar. Each would possess the general requirements outlined in Fig. 21. In brief, this system would require all the usual strain gage signal conditioning circuitry. In addition, the three signals must be converted to digital form and relayed to the host microprocessor system. Once within the microprocessor, the information can be displayed for local use or stored for future use. In the stand-alone version, the only function of the computer is to perform the basic data manipulations and to display results. In the case of CNC system interface, this information must be transferred to the host computer via a communicator bus.

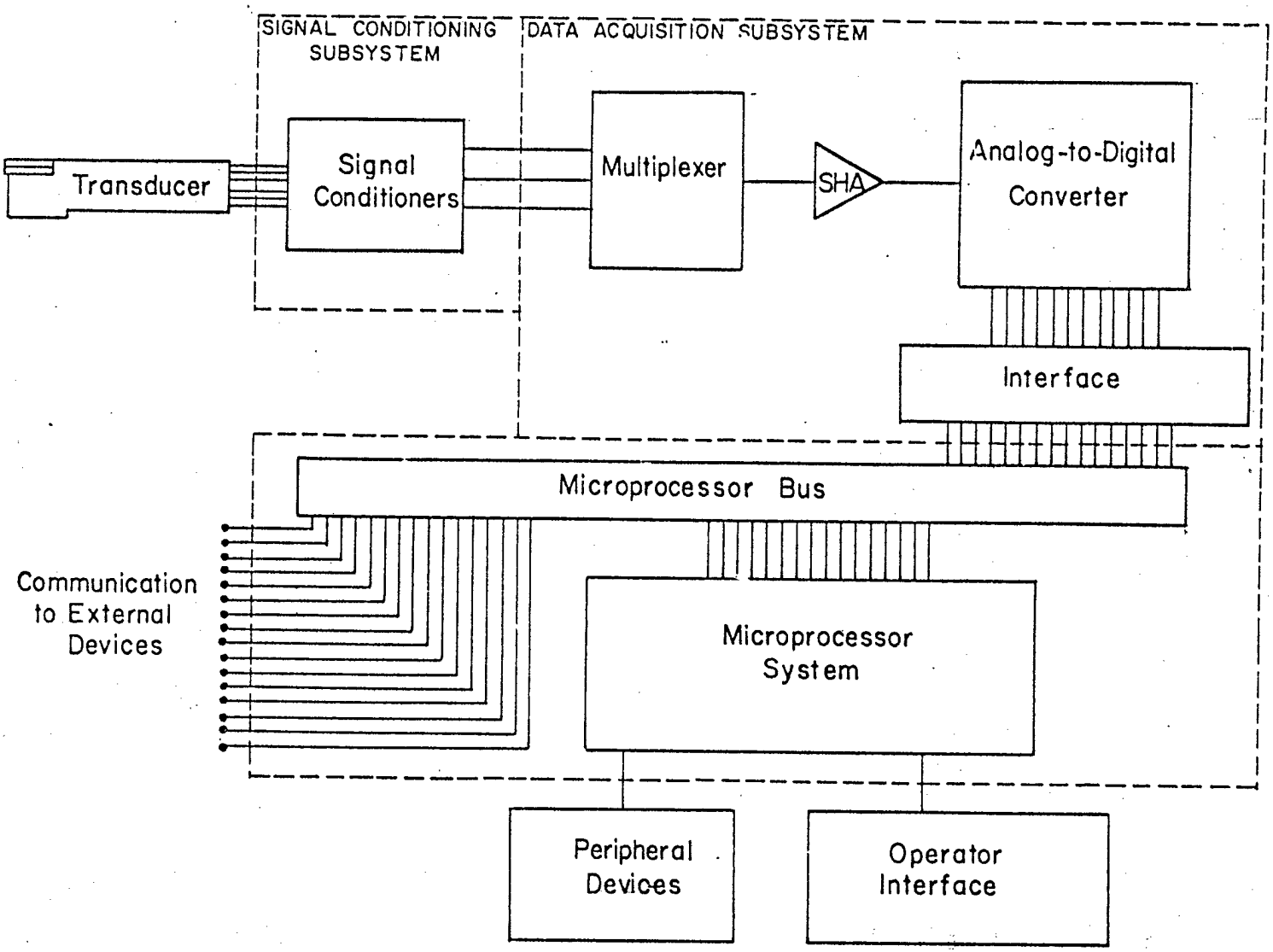


FIGURE 21: BASIC DESIGN OF DIGITAL SIGNAL PROCESSING SYSTEM

# 9. CONCLUSIONS

The major conclusions of this Phase I program are as follows:

1. An analytical model was developed which accurately predicts the magnitude of strain signals on an instrumented toolholder

2. A standard toolholder can be instrumented to provide accurate force signals in horizontal and vertical plane. Additional work is required to measure axial force.

3. Matrix methods for reducing mechanical crosstalk from one force to another are effective. The prototype signal processing scheme demonstrated this result.

4. Additional research is required to create a three axis instrumented toolholder and to interpret the force signals so that they are useable in an adaptive control scheme.

REFERENCES


1. Roark, R. J., Young, W. C., Formulas for Stress and Strain, McGraw-Hill, 1975.

2. Langhammer, K., "Cutting Forces as Parameters for Determining Wear on Carbide Lathe Tools and as Machinability Criterion for Steel," The Carbide Journal, May-June 1976.

3. Colwell, L. V., "Methods for Sensing the Rate of Tool Wear," Annals of the C.I.R.P., Vol. XVIV, pp. 647-651.

4. H. Takeyama, Y. Doi, T. Mitsuoka and H. Sekiguchi, Mechanical Engineering Laboratory, Japan, "Sensors of Tool Life for Optimization of Maching Advances in Machine Tool Design and Research", Proceedings of the 8th Int'l. M.T.D.R. Conference, Pergamon Press, New York, 1967.

5. Semiconductor Strain Gage Handbook, BLH Corp., Waltham, Mass, Dec. 1973.

# APPENDIX A

## DETAILED ANALYTICAL MODEL OF INSTRUMENTED TOOLHOLDER

Figure A.1 shows one method of locating gages to optimize sensitivity and minimize crosstalk. In this appendix we ahall present the details of an analytical model for predicting the output of these strain gages wired in a four-arm-bridge configuration.

We shall begin by modeling this toolholder as a cantilever beam clamped a distance L from the cutting point. This beam experiences a force whose components $F_p$, $F_q$ and $F_r$ act at a point with coordinates x = a and y = c. We begin the analysis by writing expressions for the moments about each axis as

$$\begin{aligned} M_x &= F_p l + F_r a \\ M_y &= F_r c - F_q l \\ M_z &= F_p c - F_q a. \end{aligned} \qquad \text{A-1}$$

For each gage site we can write

$$\epsilon_n = \frac{M_x Y_n}{EI_x} + \frac{M_y X_n}{EI_{yy}} - \frac{F_r}{EA_{csx}} \qquad \text{A-2}$$

where:

$X_n$, $Y_n$ = x, y coordinates of each gage

$I_{xx}$, $I_{yy}$ = moments of inertia

E = modulus of elasticity

$A_{csx}$ = crosssectional area of the beam

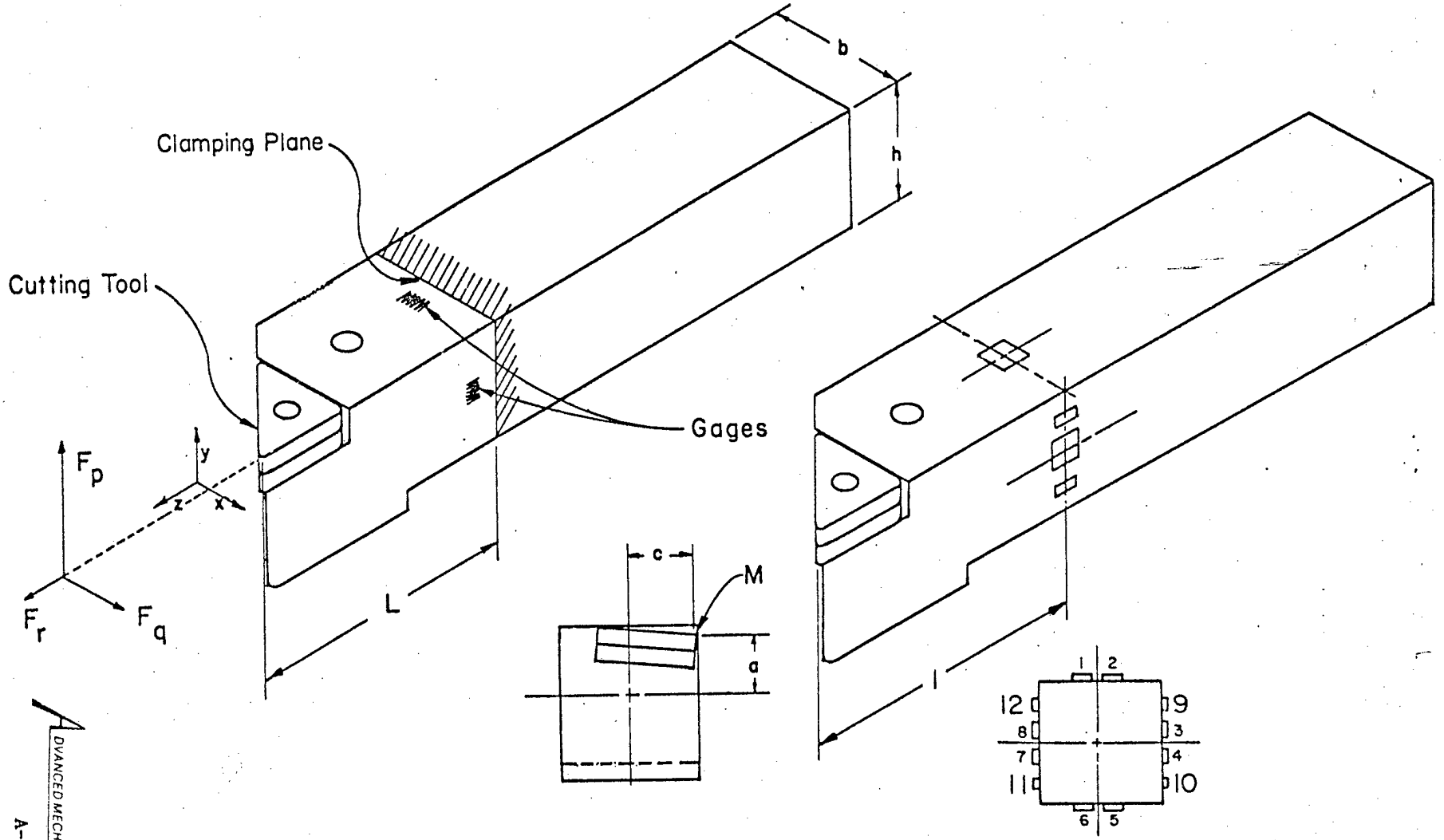


FIGURE A-1: TOOLHOLDER AND GAGE LOCATION GEOMETRY

The first two terms on the right-hand-side are the strains due to bending moments and the third term is compressive strain due to the axial force $F_r$.

Substituting Equations A-1 into A-2, we find

$$\varepsilon_n = \frac{(F_p l + F_r a) y_n}{EI_{xx}} + \frac{(F_r c - F_q l) x_n}{EI_{yy}} - \frac{F_r}{EA_{csx}} \qquad \text{A-3}$$

Rearranging, we arrive at an expression relating each strain to the three force components.

$$\varepsilon_n = \frac{l y_n}{EI_{xx}} F_p + \frac{-l x_n}{EI_{yy}} F_q + \left( \frac{a y_n}{EI_{xx}} + \frac{c x_n}{EI_{yy}} - \frac{1}{EA_{csx}} \right) F_r \qquad \text{A-4}$$

Now, by choosing gage sites and toolholder goemetry, we can substitute these values into Eq. A-4 and arrive at expressions relating strain at a point to three force components. As our example, we shall choose the case illustrated in Fig. A-2. There, we have twelve gages located on the sides and top of the toolholder. In this case, we have

$$I_{xx} = \frac{1}{12} b h^3$$
$$I_{yy} = \frac{1}{12} h b^3 \qquad \text{A-5}$$

Substituting the values for x-y coordinates into Eq. A-4, we arrive at the following matrix expression:

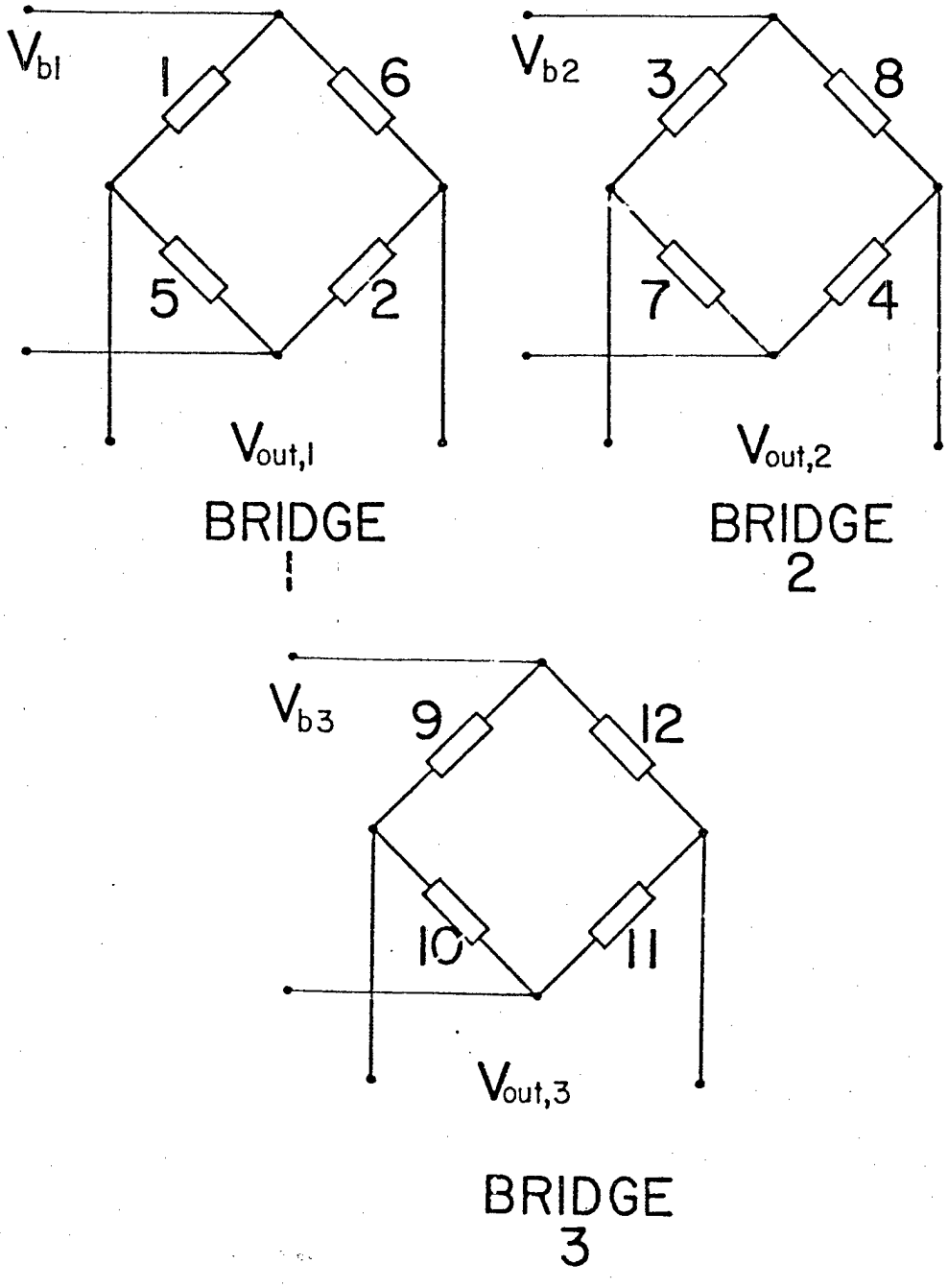


FIGURE A-2: STRAIN GAGE BRIDGE CONFIGURATIONS FOR GAGE POSITIONS PICTURED IN FIG. A-1.

$$
\begin{bmatrix} \varepsilon_1 \\ \varepsilon_2 \\ \varepsilon_3 \\ \varepsilon_4 \\ \varepsilon_5 \\ \varepsilon_6 \\ \varepsilon_7 \\ \varepsilon_8 \\ \varepsilon_9 \\ \varepsilon_{10} \\ \varepsilon_{11} \\ \varepsilon_{12} \end{bmatrix} = \frac{1}{Ebh} \begin{bmatrix} \frac{-6l}{h} & \frac{-12lx_1}{b^2} & \frac{-6a}{h} + \frac{12cx_1}{b^2} - 1 \\ \frac{-6l}{h} & \frac{-12lx_2}{b^2} & \frac{-6a}{b} + \frac{12cx_2}{b^2} - 1 \\ \frac{-12lx_3}{h^2} & \frac{-6l}{b} & \frac{-12\,y_5}{h^2} + \frac{6c}{b} - 1 \\ \frac{-12ly_4}{h^2} & \frac{-6l}{b} & \frac{-12ay_4}{h^2} + \frac{bc}{b} - 1 \\ \frac{6l}{h} & \frac{-12lx_5}{b^2} & \frac{6a}{b} + \frac{12cx_5}{b^2} - 1 \\ \frac{6l}{h} & \frac{-12lx_6}{b^2} & \frac{6a}{b} + \frac{12cx_6}{b^2} - 1 \\ \frac{-12ly_7}{h^2} & \frac{6l}{b} & \frac{-12ay_7}{h^2} - \frac{6c}{b} - 1 \\ \frac{-12ly_8}{h^2} & \frac{6l}{b} & \frac{-12ay_8}{h^2} - \frac{6c}{b} - 1 \\ \frac{-12ly_9}{h^2} & \frac{6l}{b} & \frac{-12ay_9}{h^2} + \frac{6c}{b} - 1 \\ \frac{-12ly_{10}}{h^2} & \frac{-6l}{b} & \frac{-12ay_{10}}{h^2} + \frac{6c}{b} - 1 \\ \frac{-12ly_{11}}{h^2} & \frac{6l}{b} & \frac{-12ay_{11}}{h^2} - \frac{6c}{b} - 1 \\ \frac{-12ly_{12}}{h^2} & \frac{6l}{b} & \frac{-12ay_{12}}{h^2} - \frac{6c}{b} - 1 \end{bmatrix} \begin{bmatrix} F_p \\ F_q \\ F_r \end{bmatrix} \qquad \text{A-6}
$$

These twelve strain gages can be wired together in three Wheatstone bridges as shown in Fig. A-2. An analysis of this bridge configuration shows that, for small strains, the bridge outputs are slightly non-linear with errors on the order of $(1/2\ \varepsilon^2)$. Since the strains are extremely small ($\sim 10^{-5}$), the nonlinearities become exceedingly negligible for any engineering purposes. Output from these bridges can be written

$$V_1 = \frac{V_{b_1}}{4} \quad (S_1\varepsilon_1 + S_2\varepsilon_2 - S_5\varepsilon_5 - S_6\varepsilon_6)$$

$$V_2 = \frac{V_{b_2}}{4} \quad (S_3\varepsilon_3 + S_4\varepsilon_4 - S_7\varepsilon_7 - S_8\varepsilon_8) \qquad \text{A-7}$$

$$V_3 = \frac{V_{b_3}}{4} \quad (S_9\varepsilon_9 + S_{10}\varepsilon_{10} - S_{11}\varepsilon_{11} - S_{12}\varepsilon_{12})$$

where $S_1$-$S_{12}$ are the twelve gage factors and $V_{b_1}$-$V_{b_3}$ are bridge excitation voltages.

Eq. A-6 and A-7 can be combined to yield a result of the form

$$\begin{bmatrix} V_1 \\ V_2 \\ V_3 \end{bmatrix} = [B] \begin{bmatrix} F_p \\ F_q \\ F_r \end{bmatrix} \qquad \text{A-8}$$

Eq. A-8, then, is a matrix representation relating three bridge outputs to three force inputs. If one were to premultiply both sides of A-8 by $[B]^{-1}$, one would obtain

$$[F]=[B]^{-1}[V] \ . \qquad \text{A-9}$$

# APPENDIX B

## LISTING OF COMPUTER CODING OF ANALYTICAL MODEL

```
00010 C***THIS SUBROUTINE CALCULATES THE INFLUENCE MATRIX
00020       SUBROUTINE AIJ
00030       COMMON /INFMAT/AMATRX
00040       COMMON/GEOM/H,L,B,A,C,E
00050       COMMON/GAGPOS/X1,X2,Y3,Y4,X5,X6,Y7,Y8,Y9,Y10
00060       REAL L,AMATRX(10,3)
00070       AMATRX(1,1)=-6.*L/H
00080       AMATRX(1,2)=-12.*L*X1/(B*B)
00090       AMATRX(1,3)=(-6.*A*H)+(12.*C*X1/(B*B))-1.0
00110       AMATRX(2,1)=AMATRX(1,1)
00120       AMATRX(2,2)=-12.*L*X2/(B*B)
00130       AMATRX(2,3)=(-6.*A*H)+(12.*C*X2/(B*B))-1.0
00140       AMATRX(3,1)=-12.*L*Y3/(H*H)
00150       AMATRX(3,2)=-6.*L/B
00160       AMATRX(3,3)=(-12.*A*Y3/(H*H))+(6.*C/B)-1.0
00170       AMATRX(4,1)=-12.*L*Y4/(H*H)
00180       AMATRX(4,2)=AMATRX(3,2)
00190       AMATRX(4,3)=(-12.*A*Y4/(H*H))+(6*C/B)-1.0
00200       AMATRX(5,1)=-AMATRX(1,1)
00210       AMATRX(5,2)=-12.*L*X5/(B*B)
00220       AMATRX(5,3)=(6.*A/H)+(12.*C*X5/(B*B))-1.0
00230       AMATRX(6,1)=AMATRX(5,1)
00240       AMATRX(6,2)=-12.*L*X6/(B*B)
00250       AMATRX(6,3)=(6.*A/H)+(12. *C*X6/(B*B))-1.0
00260       AMATRX(7,1)=-12.*L*Y7/(H*H)
00270       AMATRX(7,2)=-AMATRX(3,2)
00280       AMATRX(7,3)=(-12.*A*Y7)-(6.*C/B)-1.0
00290       AMATRX(8,1)=-12.*L*Y8/(H*H)
00300       AMATRX(8,2)=AMATRX(7,2)
00310       AMATRX(8,3)=(-12.*A*Y8)-(6.*C/B)-1.0
```

```
00320       AMATRX(9,1)=-12.*L*Y9/(H*H)
00330       AMATRX(9,2)=AMATRX(3,2)
00340       AMATRX(9,3)=(-12.*A*Y9/(H*H))+(6.*C/B)-1.0
00350       AMATRX(10,1)=-12.*L*Y10/(H*H)
00360       AMATRX(10,2)=-AMATRX(9,2)
00370       AMATRX(10,3)=(-12.*A*Y10/(H*H))-(6.*C/B)-1.0
00380 C***MULTIPLY BY COMMON TERM
00390       DO 50 I=1,10
00400       DO 50 J=1,3
00410       AMATRX(I,J)=AMATRX(I,J)/(E*B*H)
00420    50 CONTINUE
00430       RETURN
00440       END
00450 C***THIS MAINLINE SIMPLY CALCULATES STRAINS FROM INPUTS
00460       REAL L,AMATRX(10,3),FORCE(3),STRAIN(10),ATTN(3,3),VA(3),VF(3)
00462       REAL S(10),VBROUT(3)
00480 C*** AND OUTPUTS RESULTS.
00490       REAL L
00500       NAMELIST/GEOMIN/H,L,B,A,C,E,X1,X2,Y3,Y4,X5,X6,Y7,Y8,Y9,Y10
00510       NAMELIST/FORCES/FORCE/GFACTR/S/POTSET/ATTN/GAINS/H1,H2,H3
00520       NAMELIST/BRIDGE/VBROUT,VB1IN,VB2IN,VB3IN
00530       NAMELIST/OUTDAT/AMATRX,STRAIN
00540       COMMON /INFMAT/AMATRX
00550       COMMON/GEOM/H,L,B,A,C,E
00560       COMMON/GAGPOS/X1,X2,Y3,Y4,X5,X6,Y7,Y8,Y9,Y10
00562       COMMON/VRATV/STRAIN,S
00580 C***READ INPUT DATA FROM FILE 10
00582       WRITE(6,8888)
00584  8888 FORMAT(' PLEASE ADVANCE PAPER TO TOP OF NEXT PAGE.......')
00586       READ(5,8889)ADUMMY
```

```
00588  8889 FORMAT(1A1)
00590    10 CONTINUE
00600       READ(10,GEOMIN,END=500)
00610       READ(10,GEOMIN)
00615       READ(10,GEOMIN)
00620       READ(10,FORCES)
00630       READ(10,GFACTR)
00640       READ(10,FOTSET)
00650       READ(10,GAINS)
00660       READ(10,BRIDGE)
00670 C***DETERMINE INFLUENCE MATRIX
00680       CALL AIJ
00690 C***ZERO STRAIN MATRIX
00700       DO 50 I=1,10
00710    50 STRAIN(I)=0.0
00720 C***CALCULATE STRAINS
00730       DO 100 I=1,10
00740       DO 100 J=1,3
00750       STRAIN(I)=STRAIN(I)+AMATRX(I,J)*FORCE(J)
00760   100 CONTINUE
00770 C***CALCULATE BRIDGE OUTPUTS
00780       VBROUT(1)=VB1IN*(VRAT(1,5)-VRAT(6,2))
00790       VBROUT(2)=VB2IN*(VRAT(3,8)-VRAT(7,4))
00800       VBROUT(3)=VB3IN*((1./(2.+S(10)*STRAIN(10)))-(1.+S(9)*STRAIN(9))
00810      1/(2.+S(9)*STRAIN(9)))
00820       VA(1)=VBROUT(1)*H1
00830       VA(2)=VBROUT(2)*H2
00840       VA(3)=VBROUT(3)*H3
00850 C***ZERO OUTPUT MATRIX
00860       DO 700 J=1,3
```

```
00870   700 VF(J)=0.00000
00880 C***CALCULATE VOLTAGE OUTPUITS
00890       DO 800 I=1,3
00900       DO 800 J=1,3
00910       VF(I)=VF(I)+VA(J)*ATTN(I,J)
00920   800 CONTINUE
00930 C***OUTPUT RESULTS
00932       WRITE(6,9999)
00940       WRITE(6,GEOMIN)
00950       WRITE(6,FORCES)
00960       WRITE(6,POTSET)
00970       WRITE(6,BRIDGE)
00980       WRITE(6,GAINS)
00982       WRITE(6,2222)
00984       WRITE(6,2222)
00990       WRITE(6,1000)
01000       WRITE(6,1001)((STRAIN(I),AMATRX(I,1),AMATRX(I,2),AMATRX(I,3),FORC
01010      1(I)),I=1,3)
01020       WRITE(6,1002)((STRAIN(I),AMATRX(I,1),AMATRX(I,2),AMATRX(I,3)),I=4
01030      110)
01040       WRITE(6,2222)
01050       WRITE(6,1500)
01060       WRITE(6,1001)((VF(I),ATTN(I,1),ATTN(I,2),ATTN(I,3),VA(I)),I=1,3)
01062       WRITE(6,9999)
01064  9999 FORMAT(9(/))
01070  1000 FORMAT(T8,'STRAINS',T30,'INFLUENCE MATRIX',T65,'FORCES'//)
01080  1001 FORMAT(T7,E9.3,T23,E9.3,2X,E9.3,2X,E9.3,T65,F6.1)
01090  1002 FORMAT(T7,E9.3,T23,E9.3,2X,E9.3,2X,E9.3)
01100  2222 FORMAT(2(/))
01110  1500 FORMAT(T8,'SYSTEM OUTPUTS',T30,'POT SETTINGS',T65,'AMP. OUTPUTS')
```

```
01120          GO TO 10
01130    500 CONTINUE
01140          STOP
01150          END
01160          FUNCTION VRAT(I,J)
01170          COMMON/VRATV/STRAIN(10),S(10)
01176          VRDUM=(1.+S(I)*STRAIN(I))/(2.+S(I)*STRAIN(I)+S(J)*STRAIN(J))
01177          VRAT=VRDUM
01180          RETURN
01190          END
END OF DATA
```

# APPENDIX C

## TABULATION OF ANALYTICAL RESULTS

| STRAINS | INFLUENCE MATRIX | | | FORCES |
|---|---|---|---|---|
| 0.102E-03 | -.104E-05 | 0.145E-06 | -.365E-06 | -100.00 |
| 0.893E-04 | -.104E-05 | -.145E-06 | -.287E-06 | 50.00 |
| -.335E-04 | -.145E-06 | -.104E-05 | 0.153E-06 | 25.00 |
| -.609E-04 | 0.145E-06 | -.104E-05 | 0.218E-06 | |
| -.106E-03 | 0.104E-05 | -.145E-06 | 0.180E-06 | |
| -.939E-04 | 0.104E-05 | 0.145E-06 | 0.102E-06 | |
| 0.289E-04 | 0.145E-06 | 0.104E-05 | -.338E-06 | |
| 0.563E-04 | -.145E-06 | 0.104E-05 | -.403E-06 | |
| 0.334E-05 | -.536E-06 | -.104E-05 | 0.646E-07 | |
| -.978E-04 | 0.536E-06 | -.104E-05 | 0.306E-06 | |
| -.797E-05 | 0.536E-06 | 0.104E-05 | -.250E-06 | |
| 0.932E-04 | -.536E-06 | 0.104E-05 | -.491E-06 | |

| | | | |
|---|---|---|---|
| | -.209E-01 | 0.0 | -.470E-02 |
| B-MATRIX: | 0.0 | -.209E-01 | 0.560E-02 |
| | 0.0 | 0.0 | -.324E-01 |

| F(CALC) | B-INVERSE | | | BRIDGE OUTPUT |
|---|---|---|---|---|
| -100.00 | -.479E+02 | 0.0 | 0.694E+01 | 1.972 |
| 50.00 | 0.0 | -.479E+02 | -.827E+01 | -0.905 |
| 25.00 | 0.0 | 0.0 | -.309E+02 | -0.810 |

| STRAINS | INFLUENCE MATRIX | | | FORCES |
|---|---|---|---|---|
| 0.102E-03 | -.104E-05 | 0.145E-06 | -.365E-06 | -100.00 |
| 0.893E-04 | -.104E-05 | -.145E-06 | -.287E-06 | 50.00 |
| -.335E-04 | -.145E-06 | -.104E-05 | 0.153E-06 | 25.00 |
| -.609E-04 | 0.145E-06 | -.104E-05 | 0.218E-06 | |
| -.106E-03 | 0.104E-05 | -.145E-06 | 0.180E-06 | |
| -.939E-04 | 0.104E-05 | 0.145E-06 | 0.102E-06 | |
| 0.289E-04 | 0.145E-06 | 0.104E-05 | -.338E-06 | |
| 0.563E-04 | -.145E-06 | 0.104E-05 | -.403E-06 | |
| 0.334E-05 | -.536E-06 | -.104E-05 | 0.646E-07 | |
| -.150E-04 | 0.270E-06 | 0.226E-06 | 0.241E-07 | |
| -.797E-05 | 0.536E-06 | 0.104E-05 | -.250E-06 | |
| 0.162E-04 | -.270E-06 | -.226E-06 | 0.241E-07 | |

| | | | |
|---|---|---|---|
| | -.209E-01 | 0.0 | -.470E-02 |
| B-MATRIX: | 0.0 | -.209E-01 | 0.560E-02 |
| | 0.0 | 0.0 | -.235E-01 |

| F(CALC) | B-INVERSE | | | BRIDGE OUTPUT |
|---|---|---|---|---|
| -100.00 | -.479E+02 | 0.0 | 0.957E+01 | 1.972 |
| 50.00 | 0.0 | -.479E+02 | -.114E+02 | -0.905 |
| 25.00 | 0.0 | 0.0 | -.425E+02 | -0.588 |

| STRAINS | INFLUENCE MATRIX | | | FORCES |
|---|---|---|---|---|
| 0.102E-03 | -.104E-05 | 0.145E-06 | -.365E-06 | -100.00 |
| 0.893E-04 | -.104E-05 | -.145E-06 | -.287E-06 | 50.00 |
| -.335E-04 | -.145E-06 | -.104E-05 | 0.153E-06 | 25.00 |
| -.609E-04 | 0.145E-06 | -.104E-05 | 0.218E-06 | |
| -.106E-03 | 0.104E-05 | -.145E-06 | 0.180E-06 | |
| -.939E-04 | 0.104E-05 | 0.145E-06 | 0.102E-06 | |
| 0.289E-04 | 0.145E-06 | 0.104E-05 | -.338E-06 | |
| 0.563E-04 | -.145E-06 | 0.104E-05 | -.403E-06 | |
| 0.334E-05 | -.536E-06 | -.104E-05 | 0.646E-07 | |
| -.150E-04 | 0.270E-06 | 0.226E-06 | 0.241E-07 | |
| -.797E-05 | 0.536E-06 | 0.104E-05 | -.250E-06 | |
| 0.162E-04 | -.270E-06 | -.226E-06 | 0.241E-07 | |

| | | | |
|---|---|---|---|
| B-MATRIX: | -.209E-01 | 0.0 | -.470E-02 |
| | 0.0 | -.209E-01 | 0.560E-02 |
| | 0.0 | 0.0 | -.204E-01 |

| F(CALC) | B-INVERSE | | | BRIDGE OUTPUT |
|---|---|---|---|---|
| -100.00 | -.479E+02 | 0.0 | 0.110E+02 | 1.972 |
| 50.00 | 0.0 | -.479E+02 | -.131E+02 | -0.905 |
| 25.00 | 0.0 | 0.0 | -.490E+02 | -0.510 |

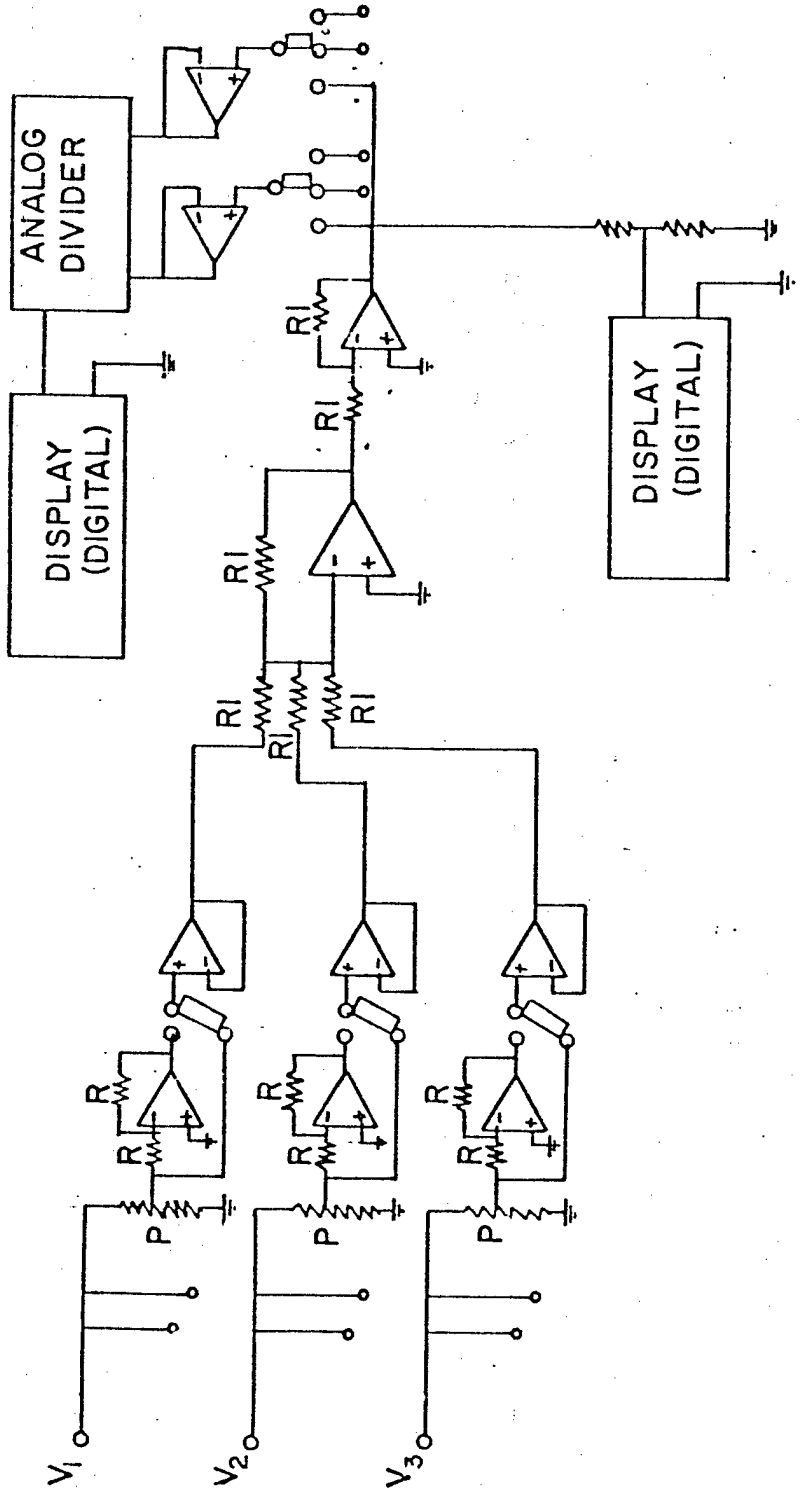


APPENDIX D: CIRCUIT DIAGRAM OF ONE CHANNEL OF SIGNAL PROCESSING SYSTEM